united nations
educational, scientific
and cultural
organization

international atomic
energy agency

the
abdus salam
international centre for theoretical physics

SMR/1270-9

SCHOOL ON SYNCHROTRON RADIATION

6 November – 8 December 2000

Miramare - Trieste, Italy

Supported in part by the Italian Ministry of Foreign Affairs in connection with the SESEME project

Co-sponsors: Sincrotrone Trieste, Società Italiana di Luce di Sincrotrone (SILS) and the Arab Fund for Economic and Social Development

Electromagnetic Radiation from Relativistic Electron Beams

H. Wiedemann
Stanford University
CA - USA

Electromagnetic Radiation from Relativistic Electron Beams

Helmut Wiedemann
Stanford University

School on Synchrotron Radiation
November 13-16, 2000
Abdus Salam Int. Center for Theoretical Physics, ICTP
Trieste, Italy

Abstract

These notes represent an introduction to the physics of synchrotron radiation. Such radiation is produced by relativistic electron beams being deflected by magnetic field. Specifically, relativistic electron beams are injected into circular accelerators, called *storage rings*, where they circulate for many hours while continuously producing synchrotron radiation for the benefit of research in pure and applied science. In another note "Introduction to Storage Ring Physics" the basic workings of storage rings are discussed. Here we concentrate on the more detailed discussion of the characteristics of synchrotron radiation. Furthermore, we discuss the characteristics of insertion-device radiation like that from undulator and wiggler magnets. The format of this note is too short to cover much detail and therefore many results are given without derivation. Interested readers are pointed to the books "Particle Accelerator Physics", Vol. I and II by H. Wiedemann, Springer Verlag for more detailed discussions.

1 History

Ever since J.C. Maxwell formulated his unifying electro-magnetic theory in 1873, the phenomenon of electromagnetic radiation has fascinated the minds of theorists as well as experimentalists. The idea of displacement currents was as radical as it was important to describe electromagnetic waves. It was only fourteen years later when G. Hertz in 1887 succeeded to generate, emit and receive again electromagnetic waves, thus, proving experimentally the existence of electromagnetic waves and the validity of Maxwell's equations. The sources of electromagnetic radiation are oscillating electric charges and currents in a system of metallic wires.

Conceptually it was also only logic to expect electromagnetic waves to be emitted from free oscillating charges as well. Mathematically, however, significant problems appeared in the formulation of the radiation field from free charges. It became obvious that the radiation field at the observation point would depend on the dynamics of all radiating charges not at the time of observation but rather at the time the observed fields were emitted due to the finite speed of propagation of electromagnetic fields. It was Liénard in 1898 and independently in 1900 Wiechert who were first to formulate the concept of retarded potentials, now called the *Liénard-Wiechert potentials* for point charges like electrons. These retarded potentials relate the scalar and vector potential of electromagnetic fields at the observation point to the location of the emitting charges and currents at the time of emission. Using these potentials, Liénard was able to calculate the energy lost by electrons while circulating in a homogenous magnetic field.

Schott formulated and published in 1907 his classical theory of radiation from an electron circulating in a homogenous magnetic field. Although he was mainly interested in the spectral distribution of radiation and hoped to find an explanation for atomic radiation spectra. Verifying Liénard's conclusion on the energy loss he derived the angular and spectral distribution and the polarization of the radiation. Since this attempt to explain atomic spectra failed his paper was basically forgotten and many of his findings have been rediscovered forty years later.

The theory of electromagnetic radiation from free electrons became fashionable again in the mid forties in parallel with the successful development of circular high-energy electron accelerators. At this time powerful betatrons have been put into operation and it was Ivanenko and Pomeranchouk who first in 1944 pointed out a possible limit to the betatron principle and maximum energy due to energy loss to electromagnetic radiation. This prediction was used by Blewett to calculate the radiation energy loss per turn in a newly constructed 100 MeV betatron at General Electric and to derive the change in the electron beam orbit due to this energy loss. In 1946 he measured the shrinkage of the orbit due to radiation losses and the results agreed with predictions. On April 24, 1947 visible radiation was observed for the first time at the 70 MeV synchrotron built at General Electric. Since then this radiation is called *synchrotron radiation.*

The energy loss of particles to synchrotron radiation causes technical and economic limits for circular electron or positron accelerators. As the particle energy is driven higher and higher, more and more rf power must be supplied to the beam not only to accelerate particles but also to overcome energy losses due to synchrotron radiation. The limit is reached when the radiation power grows to high enough levels exceeding technical cooling capabilities or exceeding the funds available to pay for the high cost of electrical power. To somewhat ameliorate this limit, high-energy electron accelerators have been constructed with ever increasing circumferences to allow a more gentle bending of the particle beam. Since the synchrotron radiation power scales like the square of the particle energy the circumference must scale similar for a constant amount of rf power. Usually a compromise is reached by increasing the circumference less and adding more rf power in spaces along the ring lattice made available by the increased circumference. In general the maximum energy in large circular electron accelerators is limited by the available rf power while the maximum energy of proton or ion accelerators and low energy electron accelerators is more likely limited by the maximum achievable magnetic fields in bending magnets.

What is a nuisance for one group of researchers can be a gift for another group. Synchrotron radiation is emitted tangentially from the particle orbit and within a highly collimated angle of $\pm 1/\gamma$. The spectrum reaches from radio frequencies up to photon energies of many thousand electron volts, the radiation is polarized and the intensities greatly exceed most other available radiation sources specifically in the vacuum ultra violet to x-ray region.

With these properties synchrotron radiation was soon recognized to be a powerful research tool for material sciences, crystallography, surface physics, chemistry, biophysics, and medicine to name only a few areas of research. While in the past most of this research was done parasitically on accelerators built and optimized for high-energy physics the usefulness of synchrotron radiation for research has become important in its own right to justify the construction and operation of dedicated synchrotron radiation sources all over the world.

2 Emission of Electromagnetic Radiation

Charged particles do not radiate while in uniform motion, but during acceleration a rearrangement of its electric fields is required and this field perturbation, travelling away from the charge at the velocity of light, is what we observe as electromagnetic radiation. Such emission occurs, for example, in a radio or TV antenna where electric charges are periodically driven up and down the antenna at the carrier frequency specific for the station. Free accelerated electrons radiate similarly, although now the source (antenna) is moving. Radiation from a fast moving particle source appears to the observer in the laboratory as being all emitted in the general direction of motion of the particle. Think of tomatoes being thrown in all directions from a fast moving truck. This forward collimation is particularly effective for highly relativistic electrons where most of the radiation is concentrated in a small cone with an opening angle of $1/\gamma$

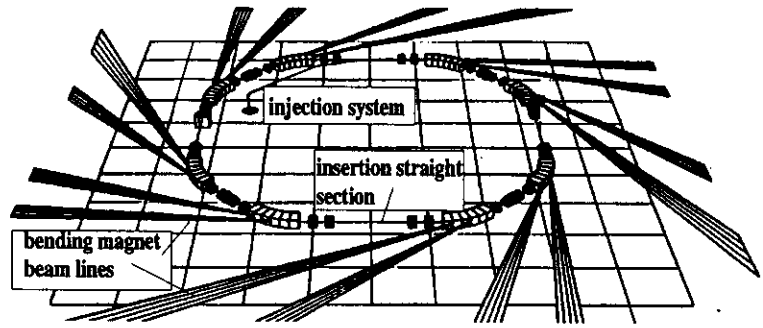

Figure 1: Schematic layout od a synchrotron light source

(some 0.1 to 1 mrad), where γ is the particle energy in units of its rest energy (typically of the order of $10^3 - 10^4$). In synchrotron radiation sources (storage rings) highly relativistic electrons are stored to travel along a circular path for many hours. Radiation is caused by transverse acceleration due to magnetic forces in bending magnets (forming the circular path) or periodic acceleration in special insertion device magnets like undulators, wiggler magnets and wave length shifters. In Fig. 1 a schematic layout is shown for a typical synchrotron radiation source in form of a storage ring. Particles orbit in a circular accelerator and emit synchrotron radiation as they get deflected while passing through bending magnets. Through specially designed openings in the vacuum chamber small slices of radiation emerge from the storage ring and to be guided to experimental stations.

Radiation is linearly polarized in the plane of acceleration (this is in most cases the horizontal plane). Elliptical polarization occurs for bending magnet radiation observed above or below the midplane. The radiation is emitted in pulses of 10 - 20 p-sec separated by some 2 nsec or longer separation if desired.

3 Radiation Sources

Bending Magnet: Radiation is emitted tangentially to the orbit similar to a search light. Due to the high collimation in the forward direction the observer sees radiation from only a small fraction of the circular path which can be described as a piece of a distorted sinusoidal motion. The extremely short duration of the light pulse at the location of the observer provides a broad spectrum of radiation. The field of a ring bending magnet cannot be chosen freely because these magnets form the geometry of the storage ring and the radiation characteristics are therefore fixed. To obtain some flexibility in the characterisitics of the radiation insertion devices are used as radiation sources. Such devices are installed in ring-magnet free sections and must not introduce

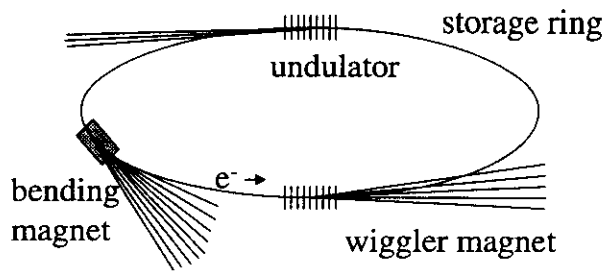

Figure 2: Synchrotron radiation sources in a storage ring. Wide, broadband bending magnet radiation, well collimated, broadband wiggler radiation and highly collimated, monochromatic undulator radiation

a net deflection to the particle beam. generally, a set of magnet poles with opposite signs of the magnetic fields are employed such that the total deflection angle is zero. Within this constraint a variety of specialized photon beams can be produced. Main examples of such insertion devices will be introduced.

Wavelength Shifter: This magnet consists of a high field central pole and two weaker outside poles to compensate the deflection by the central pole. The field strength can be chosen freely to adjust the critical photon energy and is used in conjunction with superconducting magnet technology particularly in low energy rings to extend the available photon energy to higher value.

Undulator: The electron beam is periodically deflected by weak magnetic fields. Similar to antenna radiation the particle emits radiation at the wavelength of its periodic motion in the undulator. To the particle this wavelength is the undulator period length (l_p) divided by γ due to relativistic Lorentz contraction. In the laboratory system this wavelength appears to the observer further reduced by another factor γ due to the Doppler effect. The undulator period length of the order of cm's is thus reduced by a factor γ^2 (of the order of $10^6 - 10^8$) to yield short wavelength radiation in the VUV and x-ray regime. Variation of the magnetic field allows to vary this wavelength within some range. The relative spectral width of the radiation is inversely proportional to the number of undulator periods.

Wiggler Magnet: Increasing the magnetic field strength causes the pure sinusoidal transverse motion of electrons in an undulator to become distorted due to relativistic effects generating higher harmonics of the single wavelength undulator radiation. The monochromatic undulator spectrum therefore changes into a line spectrum. For very strong fields more and more harmonics are generated which eventually merge to form a continuous spectrum from IR to hard x-rays. The radiation intensity drops exponentially at photon energies

higher than the critical photon energy. The critical photon energy depends on the magnetic field strength and the third power of the particle energy. The radiation intensity multiplies with the number of wiggler magnet poles.

4 Elements of Radiation Theory

The scope of these lectures does not allow the detailed discussion of the theory of synchrotron radiation. We therefore concentrate mainly on the basic features and results of this theory. For more detailed discussions, please consult a relevant textbook.

4.1 Radiation Fields

Radiation is the perturbation of the electric field of a charged particle. Whenever a charge particle becomes accelerated the electric fields must realign themselves and it is this realignment that we call radiation. The radiation power is expressed by the Poynting vector $\mathbf{S} = \frac{c}{4\pi}[\mathbf{E} \times \mathbf{B}]$ defined as the radiation power through a unit surface element. We expect therefore to describe radiation by deriving the electromagnetic field from the dynamics of charged particles. Such electromagnetic fields can be expressed in terms of the retarded Lienard-Wiechert potentials:

$$\mathbf{A}(P,t) = \left.\frac{e}{R}\frac{\boldsymbol{\beta}}{1+\mathbf{n}\boldsymbol{\beta}}\right|_{\mathrm{r}}, \qquad \phi(P,t) = \left.\frac{e}{cR}\frac{1}{1+\mathbf{n}\boldsymbol{\beta}}\right|_{\mathrm{r}}, \tag{1}$$

where $\mathbf{R}(t_{\mathrm{r}})$ is the distance vector from the observer at point P to the radiating charged particle or source, the unit vector $\mathbf{n} = \mathbf{R}/R$. All quantities on the r.h.s. are taken at the retarded time $ct_{\mathrm{r}} = ct - R(t_{\mathrm{r}})$. This is required because the radiation field at the observer at time t is not emitted by the particles at the same time but at an earlier time, the retarded time. Location and dynamics at that time must be considered to evaluate the observed fields at time t.

From the potentials we derive the fields by some differentiation $\mathbf{E} = -\frac{\partial}{\partial t}\mathbf{A} - \nabla\phi$ and $\mathbf{B} = \nabla \times \mathbf{A}$. With $c\mathbf{B} = [\mathbf{E} \times \mathbf{n}]_{\mathrm{r}}$ the Poynting vector becomes $\mathbf{S}_{\mathrm{r}}(t) = -c^2 E^2 (1+\boldsymbol{\beta}\mathbf{n})\mathbf{n}|_{\mathrm{r}}$ and the instantaneous radiation power per unit solid angle

$$\begin{aligned}\frac{\mathrm{d}P(t)}{\mathrm{d}\Omega} &= -\mathbf{n}\mathbf{S}R^2|_{\mathrm{r}} = c^2\mathbf{E}^2(1+\boldsymbol{\beta}\mathbf{n})\,R^2|_{\mathrm{r}} \\ &= \frac{r_{\mathrm{c}}mc^2}{4\pi c}\frac{R^5}{r^5}\left|\mathbf{n}\times[(\mathbf{n}+\boldsymbol{\beta})\times\dot{\boldsymbol{\beta}}]\right|^2_{\mathrm{r}}, \end{aligned}\tag{2}$$

where $r = R(1+\mathbf{n}\boldsymbol{\beta})$. Replacing $\mathrm{d}W/\mathrm{d}\Omega = \int(\mathrm{d}P/\mathrm{d}\Omega)\mathrm{d}t$ and taking the Fourier transform of the electric field results in the spatial and spectral distribution of radiation energy emitted by one electron during a single pass:

$$\frac{\mathrm{d}^2W}{\mathrm{d}\omega\,\mathrm{d}\Omega} = \frac{r_{\mathrm{c}}mc^2}{4\pi^2 c}\omega^2 \times \left|\int_{-\infty}^{\infty}[\mathbf{n}\times[\mathbf{n}\times\boldsymbol{\beta}]]\,\mathrm{e}^{-\mathrm{i}\omega\left(t_{\mathrm{r}}+\frac{R}{c}\right)}\mathrm{d}t_{\mathrm{r}}\right|^2_{\mathrm{r}}.$$

Specific radiation characteristics are determined by the particular temporal variation of $\boldsymbol{\beta}$ and $\mathbf{n}$ along the particle path.

4.2 Radiation Power

The total radiation power per particle in its own system is

$$P^* = \frac{2r_c\, mc^2}{3c}\dot{\beta}^{*2}, \tag{3}$$

which becomes after Lorentz transformation into the laboratory system

$$P = \frac{2r_c mc^2}{3c}\gamma^2\left[\left(\frac{\mathrm{d}}{\mathrm{d}t}\gamma\beta\right)^2 - \left(\frac{\mathrm{d}\gamma}{\mathrm{d}t}\right)^2\right]. \tag{4}$$

Defining acceleration vectors parallel and orthogonal to the particle motion $\dot{\boldsymbol{\beta}} = \dot{\boldsymbol{\beta}}_{\parallel} + \dot{\boldsymbol{\beta}}_{\perp}$ splits the total radiation power into parts due to parallel and transverse acceleration respectively. Transverse acceleration is much more intense than longitudinal acceleration and we concentrate therefore only on transverse acceleration. In case of transverse deflection by magnetic fields and bending radius ρ we have $\dot{\beta}_{\perp} = \beta^2 c/\rho$ and the instantaneous radiation power is

$$P_{\perp}^{\mathrm{m}} = \tfrac{2}{3}\, c\, r_c\, mc^2\, \frac{\beta^4\gamma^4}{\rho^2}. \tag{5}$$

The radiation power depends greatly on the mass of the radiating particle scaling like $1/m^4$. For protons the radiation power compared to electrons of the same energy is

$$\frac{P_{\mathrm{p}}}{P_{\mathrm{e}}} = \left(\frac{m_{\mathrm{e}}}{m_{\mathrm{p}}}\right) = 8.80 \cdot 10^{-14}. \tag{6}$$

For proton energies of less than say 5000 - 10000 GeV there is no significant radiation.

4.3 Relativistic Transformations

We obtain crucial information on the spatial and spectral distribution of synchrotron radiation from a simple Lorentz transformation from the particle system S^* to the laboratory system S assuming that both systems move relatively to each other in the z-direction. The phase ψ of an electromagnetic wave is invariant to Lorentz transformations. If $\psi^* = 0$ in the particle system, e.g. the field goes through zero, then $\psi = 0$ also in the laboratory system. With $\psi = k\mathbf{n}\,\mathbf{r} - \omega t$ where $k = 2\pi/\lambda$, $\mathbf{n}$ the unit vector in the direction of radiation propagation and $\mathbf{r}$ the vector from an arbitrary reference point to the point of observation we have in component form the identity

$$\omega^*(n_x^* x^* + n_y^* y^* + n_z^* z^* - ct^*) = \omega(n_x x + n_y y + n_z z - c\omega t) \tag{7}$$

Applying the Lorentz transformation to the coordinates and time (x^*, y^*, z^*, t^*) and equating coefficients of (x, y, z, t) on both sides of the equation we get four equations relating the direction of radiation $\mathbf{n}$ and frequency from the particle system to the laboratory system. One of these equations is an expression for the relativistic Doppler effect

$$\omega = \omega^* \gamma (1 + \beta n_z^*) . \qquad (8)$$

The particle system or radiation source moves at a velocity $c\beta$ in the direction of emission of radiation towards the observer and therefore $\beta n_z > 0$. Any oscillation ω^* of the charged particle in its system will be observed in the laboratory system with a strong blue-shift. the frequency shift actually is close to a factor 2γ.

The other three equations define the transformation of directions:

$$n_x = \frac{n_x^*}{\gamma(1 + \beta n_z^*)} , \quad n_y = \frac{n_y^*}{\gamma(1 + \beta n_z^*)} , \quad n_z = \frac{\beta + n_z^*}{1 + \beta n_z^*} . \qquad (9)$$

Angles with respect to the z-axis transform with $n_z = \cos\Theta$ and $n_x^2 + n_y^2 = \sin^2\Theta$ etc. like

$$\sin\Theta \approx \frac{\sin\Theta^*}{\gamma(1 + \beta\cos\Theta^*)} \qquad (10)$$

Radiation emitted into all forward space ($\Theta^* \square \pi/2$) in particle system is therefore greatly collimated in the forward direction to within an angle $\Theta = \pm 1/\gamma$ in laboratory system. Both, the blue-shift and the strong collimation of radiation in the laboratory system make electromagnetic radiation from highly relativistic electron beams a valuable tool for research and development in science and technology.

5 Bending Magnet Radiation

The radiation from bending magnets is emitted tangentially from any point along the curved path and produces therefore a swath of radiation around the storage ring as shown in Fig. 3. In the vertical, nondeflecting plane, however, the radiation is very much collimated with a typical opening angle of $\pm 1/\gamma$.

Of course, radiation is not available to the user anywhere along the ring. Special photon beamlines are attached to the storage ring at particular locations letting a small fraction of the radiation swath out to experimental stations.

Bending magnets, being a part of the geometry of the storage ring, however, cannot be varied to optimize for desired photon beam characteristics. While the lower photon spectrum is well covered even for rather low energy storage rings the x-ray region requires high beam energies and/or high magnetic fields.

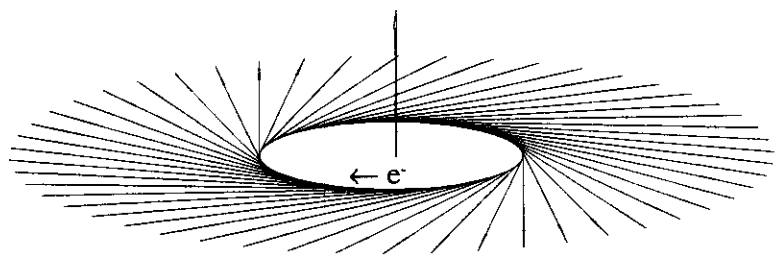

Figure 3: Synchrotron radiation swath

5.1 Synchrotron Radiation Power

The bending radius of a charged particle trajectory in a homogeneous field B at energy E is

$$\frac{1}{\rho} = \frac{eB}{\beta E} = 0.2998 \frac{B}{\beta E} \,. \tag{11}$$

and the instantaneous radiation power becomes from (5)

$$P_\gamma = \frac{c C_\gamma}{2\pi} \frac{E^4}{\rho^2} \,, \tag{12}$$

with

$$C_\gamma = \frac{4\pi}{3} \frac{r_\mathrm{c}}{(mc^2)^3} = 8.8460 \cdot 10^{-5} \frac{\mathrm{m}}{\mathrm{GeV}^3} \,, \tag{13}$$

where $r_\mathrm{c} = 2.81794 \times 10^{-15}$m is the classical electron radius. The total energy loss of each electron to radiation during a 360° orbit is

$$\Delta E = \oint P_\gamma \mathrm{d}t = \frac{C_\gamma}{2\pi} E^4 \oint \frac{\mathrm{d}s}{\rho^2} \,, \tag{14}$$

and becomes for an isomagnetic ring where all magnets are equally strong

$$\Delta E_\mathrm{iso} = C_\gamma \frac{E^4}{\rho} \,. \tag{15}$$

For a circulating beam current I the total synchrotron radiation power from all bending magnets is then

$$P_\mathrm{tot}(\mathrm{W}) = 10^9 \, C_\gamma \frac{E^4}{\rho} \frac{I}{e} \,. \tag{16}$$

As an example, an electron beam of 200 mA circulating at the LNLS ring at an energy of 1.3 GeV emits synchrotron radiation continuously at a power of 18.5 kW. Of course, this radiation is emitted tangentially to the electron orbit and is therefore distributed around the ring like the radiation from a search light.

5.2 Spectrum and Critical Photon Energy

Synchrotron radiation from relativistic charged particles is emitted over a wide spectrum of photon energies. The basic characteristics of this spectrum can be derived from simple principles. For a fixed observation point, synchrotron light has the appearance similar to the light coming from a searchlight. Although the light is emitted continuously an observer sees only a periodic flash of light as the light beam comes by. Similarly, synchrotron light emitted from relativistic particles will appear to an observer as a single flash for an electron beam passing once through a bending magnet or as a series of equidistant light flashes as bunches of particles orbit in a circular accelerator.

The duration of the light flash is very short and the observer notes a broad spectrum of frequencies as his eyes or instruments Fourier-analyze the pulse of electromagnetic energy. The spectrum of synchrotron light from a circular accelerator is composed of a large number of harmonics of the particle's revolution frequency in the circular accelerator. These harmonics reach a high frequency cutoff where the period of the radiation becomes comparable to the duration of the light pulse.

Even though the aperture of the observer's eye or instrument is assumed to be infinitely narrow we still note a finite duration of the light flash. This is a consequence of the finite opening angle of the radiation as illustrated in Fig. 4. Synchrotron light emitted by a particle travelling along the orbit cannot reach the observer before it has reached the point P_0 when those photons emitted on one edge of the radiation cone at an angle $-1/\gamma$ aim directly toward the observer. Similarly, the last photons to reach the observer are emitted from point P_1 at an angle of $+1/\gamma$. Between point P_0 and point P_1 we have therefore a deflection angle of $2/\gamma$. The duration of the light flash for the observer is not the time it takes the particle to travel from point P_0 to point P_1 but must be corrected for the time of flight for the photon emitted at P_0. If particle and photon would travel toward the observer with exactly the same velocity the light pulse would be infinitely short. However, particles move slower following a slight detour and therefore the duration of the light pulse equals the time difference between the first photons from point P_0 arriving at the observer and the last photons being emitted by the particles at point P_1. At the time $t = 0$ when the particle reaches point P_0 the first photon can be observed at point P_1 at the time

$$t_\gamma = \frac{2\rho \sin\frac{1}{\gamma}}{c}. \tag{17}$$

The last photon to reach the observer is emitted when the particle arrives at point P_1 at the time

$$t_e = \frac{2\rho}{\beta c \gamma}. \tag{18}$$

The duration of the light pulse δt is therefore given by the difference of the times

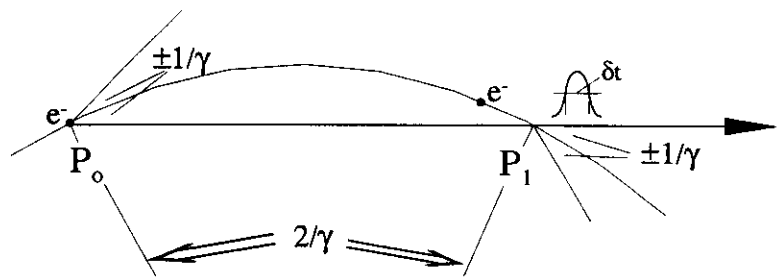

Figure 4: Time structure of synchrotron radiation

(18) and (17)

$$\delta t = t_e - t_\gamma = \frac{2\rho}{\beta c \gamma} - \frac{2\rho \sin\frac{1}{\gamma}}{c}. \tag{19}$$

The sine function can be expanded for small angles keeping linear and third order terms only and the duration of the light pulse at the location of the observer is after some manipulation

$$\delta t = \frac{4\rho}{3c\gamma^3}. \tag{20}$$

The effective pulse length is inversely proportional to the magnetic field $B \propto \gamma/\rho$ and proportional to $1/\gamma^2$ as a consequence of the *Doppler effect* since radiation is emitted from a moving source. For highly relativistic electrons this pulse length is very short leading to a spectrum that reaches far into the x-ray regime. The finite pulse length limits the expansion into Fourier harmonics and amplitudes of the spectrum drop off significantly above a frequency of about

$$\omega_{\max} \approx \frac{\pi}{\delta t} \approx \frac{3\pi}{4} c \frac{\gamma^3}{\rho}. \tag{21}$$

This is a reasonably good representation for the width of the synchrotron radiation spectrum from highly relativistic particles. In a more rigorous derivation of the spectrum the *critical photon frequency* or *critical photon energy* $\varepsilon_c = \hbar\omega_c$ is defined by

$$\omega_c = \frac{3}{2} c \frac{\gamma^3}{\rho}, \tag{22}$$

which is a convenient mathematical scaling parameter and indicates the photon frequency beyond which the intensity starts to drop significantly. Both frequencies apparently describe equally well the width of the radiation spectrum but for consistency the definition of the critical frequency is used exclusively for that purpose. In more practical units, the critical photon frequency is

$$\omega_c = C_c \frac{E^3}{\rho} \tag{23}$$

with

$$C_c = \frac{3\hbar c}{2(mc^2)^3} = 3.37 \times 10^{18} \frac{\mathrm{m}}{\mathrm{secGeV}^3}, \tag{24}$$

where the numerical value has been calculated for electrons. The critical photon energy $\epsilon_c = \hbar\omega_c$ is then given by

$$\epsilon_c(\mathrm{keV}) = 2.218 \frac{E^3(\mathrm{GeV}^3)}{\rho(\mathrm{m})} = 0.665 E^2(\mathrm{GeV}^2) B(\mathrm{Tesla}). \tag{25}$$

The synchrotron radiation spectrum from relativistic particles in a circular accelerator is made up of harmonics of the particle revolution frequency ω_o and extends to values up to and beyond the critical frequency. A real synchrotron radiation beam from say a storage ring will not display this harmonic structure. The distance between harmonics is extremely small compared to the extracted photon frequencies in the VUV and x-ray regime while the line width is finite due to the energy spread and beam emittance.

6 Spectral and Spatial Photon Distribution

The spectral and spatial distribution of photon beam from a bending magnet can be drived theoretically. The number of photons emitted per unit time and circulating beam current I at a photon energy $\epsilon_{ph} = \hbar\omega$ and bandwidth $\Delta\omega/\omega$ is given by

$$\Delta\dot{N}_{ph} = C_n E^2 I \frac{\Delta\omega}{\omega} \frac{\omega^2}{\omega_c^2} K_{2/3}^2(\xi) F(\xi,\theta) \Delta\theta \Delta\psi, \tag{26}$$

where $\Delta\theta$ is the vertical and $\Delta\psi$ the horizontal acceptance angle of the photon beam line, and $\xi = \frac{1}{2}\frac{\omega}{\omega_c}(1+\gamma^2\theta^2)^{3/2}$. The constant

$$C_n = \frac{3\alpha}{4\pi^2 e (mc^2)^2} = 1.3255 \cdot 10^{22} \frac{\mathrm{photons}}{\mathrm{sec\,rad^2\,GeV^2\,A}}, \tag{27}$$

where the electron fine structure constant $\alpha = r_e mc^2/(\hbar c)$ and

$$F(\xi,\theta) = (1+\gamma^2\theta^2)^2 \left[1 + \frac{\gamma^2\theta^2}{1+\gamma^2\theta^2} \frac{K_{1/3}^2(\xi)}{K_{2/3}^2(\xi)}\right]. \tag{28}$$

The functions $K_i^2(\xi)$ are modified Bessel's functions (Fig.5).

6.1 Spatial Power Distribution

Multiplying the differential photon flux (26) with the photon energy and integrating over all photon energies we get the spatial radiation power distribution

$$\frac{\mathrm{d}^2 P_\gamma}{\mathrm{d}\psi\,\mathrm{d}\theta} = \frac{21}{32}\frac{P_\gamma}{2\pi}\gamma \frac{1}{(1+\gamma^2\theta^2)^{5/2}} \left(1 + \frac{5}{7}\frac{\gamma^2\theta^2}{1+\gamma^2\theta^2}\right), \tag{29}$$

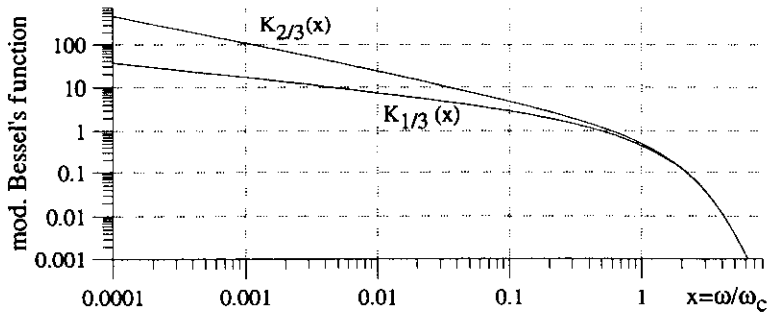

Figure 5: Functions $K_{1/3}(\xi)$ and $K_{2/3}(\xi)$

where we have introduced the radiation power P_γ form 12. The radiation power depends greatly on the vertical observation angle with an opening angle of about $\pm 1/\gamma$. In the horizontal plane we have no dependence on the angle ψ since bending magnet radiation is emitted uniformly along the tangent or the particle beam orbit.

The first term in the square bracket on the r.h.s. of (29) refers to the $\sigma-$mode polarization with the electrical field orthogonal to the deflecting field and the second term the $\pi-$mode polarization for which the electrical field is in the plane of deflecting field and line of observation. Note, that π- mode radiation is available only if the vertical observation angle $\theta \neq 0$. We also note from the common factor that the radiation is very well collimated in the vertical plane within an angle of about $\pm 1/\gamma$. In the horizontal plane (ψ) the radiation power is uniform. Integration of (29) over all angles ψ, θ gives for the two polarization modes $P_\sigma = \frac{7}{8} P_\gamma$ and $P_\pi = \frac{1}{8} P_\gamma$. Only about 12% of all radiation is in the π-mode.

6.2 Angle Integrated Photon Flux

The vertical opening angle $\pm 1/\gamma$ is often very small compared to the experimental aperture. In this case the experiment integrates the photon flux over all vertical angles θ. Integration of the photon flux (26) over all angles θ gives the total photon flux per unit horizontal deflection angle

$$\frac{\mathrm{d}\dot{N}_{\mathrm{ph}}}{\mathrm{d}\psi} = C_\psi \, E \, I \, \frac{\Delta\omega}{\omega} \, S\left(\frac{\omega}{\omega_{\mathrm{c}}}\right) , \tag{30}$$

where for electrons

$$C_\psi = \frac{4\,\alpha}{9\,e\,mc^2} = 3.9614 \cdot 10^{19} \frac{\text{photons}}{\text{sec rad A GeV}} , \tag{31}$$

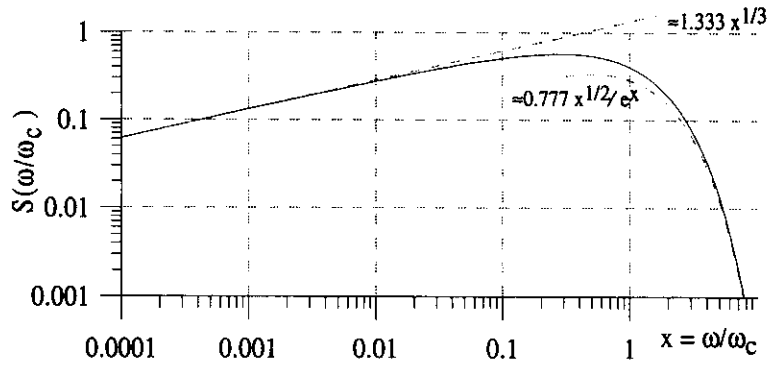

Figure 6: Universal function

and the *universal function* (Fig. 6) is defined by

$$S(\omega/\omega_c) = \frac{9\sqrt{3}}{8\pi}\frac{\omega}{\omega_c}\int\limits_{\omega/\omega_c}^{\infty} K_{5/3}(x)\,\mathrm{d}x\,. \tag{32}$$

Approximate expressions exist for $\omega \ll \omega_c$

$$\frac{\mathrm{d}\dot{N}_{\mathrm{ph}}}{\mathrm{d}\psi} \approx C_\psi\, E\, I\, \frac{\Delta\omega}{\omega}\, 1.3333 \left(\frac{\omega_{\mathrm{ph}}}{\omega_c}\right)^{\frac{1}{3}}, \tag{33}$$

and for $\omega \gg \omega_c$ with $x = \omega/\omega_c$

$$\frac{\mathrm{d}\dot{N}_{\mathrm{ph}}}{\mathrm{d}\psi} \approx C_\psi\, E\, I\, \frac{\Delta\omega}{\omega}\, 0.77736\, \frac{\sqrt{x}}{e^x}\,. \tag{34}$$

6.3 Vertical Radiation Distribution

The expressions for the photon fluxes (26) and (30) provide the opportunity to calculate the spectral distribution of the photon beam divergence. Although we derived from general principles that synchrotron radiation is emitted into an angle $\pm 1/\gamma$ this result is modified somewhat depending on the photon energy. The angular photon distribution is somehow bell-shaped and may be represented by a Gaussian distribution, at least in the core. The effective width of a Gaussian distribution is $\sqrt{2\pi}\sigma_\theta$ and we have therefore

$$\frac{\mathrm{d}\dot{N}_{\mathrm{ph}}}{\mathrm{d}\psi} \approx \frac{\mathrm{d}^2 N_{\mathrm{ph}}}{\mathrm{d}\theta \mathrm{d}\psi}\sqrt{2\pi}\sigma_\theta\,. \tag{35}$$

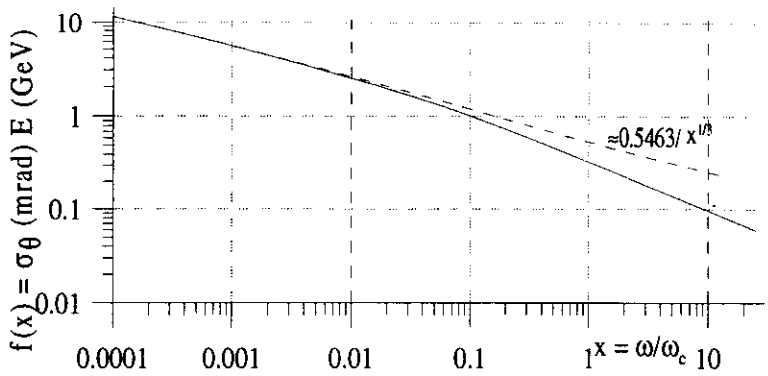

Figure 7: Vertical opening angle: $f(x) = \sigma_\theta E$

The angular divergence of the forward lobe of the photon beam

$$\sigma_\theta(\text{mrad}) = \frac{C_\psi}{\sqrt{2\pi}C_\Omega}\frac{1}{E}\frac{S(x)}{x^2K_{2/3}^2(x/2)} = \frac{f(x)}{E(\text{GeV})}, \tag{36}$$

where $x = \omega/\omega_c$. The function $f(x) = \sigma_\theta(\text{mrad})E(\text{GeV})$ valid for radiation into the forward direction $\theta \approx 0$ is shown in Fig. 7 for easy numerical calculations.

For short wavelengths $\omega \ll \omega_c$ equation (36) can be greatly simplified to become in more practical units

$$\sigma_\theta(\text{mrad}) \approx \frac{0.54626}{E(\text{GeV})}\left(\frac{\omega}{\omega_c}\right)^{1/3} = \frac{7.124}{[\rho(\text{m})\varepsilon_{\text{ph}}(\text{eV})]^{1/3}}, \tag{37}$$

where ρ is the bending radius and $\varepsilon_{\text{ph}} = \hbar\omega$ the photon energy. The photon beam divergence for low photon energies compared to the critical photon energy is independent of the particle energy and scales inversely proportional to the third root of the bending radius and photon energy. Low energy photon radiation diverges much faster than $\pm 1/\gamma$. The general variation of opening angle and frequency for both σ- and π-mode radiation can be noticed clearly in Figs. 8 and 9.

6.4 Radiation Polarization

To determine the direction of the electrical radiation field consider the electrostatic fields emanating from the electron. Upon acceleration the field lines are distorted in the direction of acceleration. Since the field lines end at a negative charge (electron) the direction of the electric field distortion is in the direction of acceleration. This distortion travels away from the charge, a process we detect as radiation. Whenever we observe a nonuniform motion of an electron from the

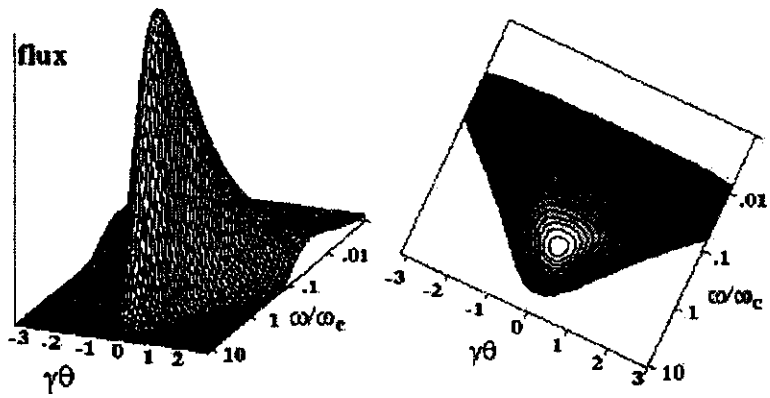

Figure 8: Spatial and spectral distribution for σ-mode radiation

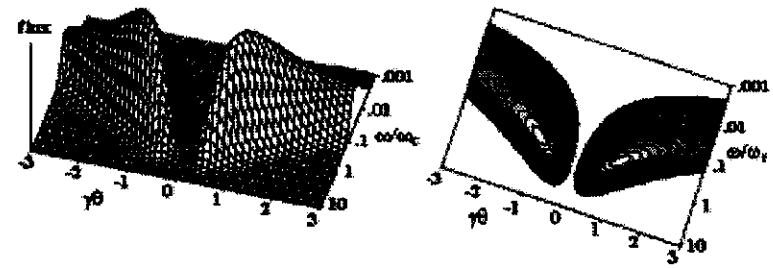

Figure 9: Spatial and spectral distribution for π-mode radiation

observation point we can also detect radiation with a specific polarization. A particle beam being deflected in the horizontal plane in a bending magnet emits synchrotron radiation which is linearly polarized in the horizontal plane when observed in the horizontal plane including the particle trajectory. This is the σ-mode polarization where the electric field is in the horizontal plane orthogonal to the deflecting magnetic field.

Viewing the particle trajectory from a point above the midplane we see the trajectory as a piece of arc. The particle appears to move now not only in the horizontal plane but follows also an up-down motion. Both motions are nonuniform and are therefore accelerated motions. We expect therefore in addition to the horizontal or σ-mode polarization also a vertical polarization which is called the π-mode. Following a particle from the top of an arc to the left and then again to the right approaching the bottom of the arc we

notice first a downward acceleration followed by an acceleration to the right and then an upward acceleration generating *elliptically polarized radiation.* If we would observe radiation from below the midplane the sequence of acceleration would be reversed and we observe radiation which is elliptical polarized in the opposite direction. In the following discussions we derive quantitative results with separate terms for both the σ- and π-mode polarization for numerical calculations.

The two terms in the square bracket of equation (28) represent the photon flux in the $\sigma-$ and $\pi-$ mode polarization respectively. The angular and spectral distribution of both modes are shown in Fig. 8 and 9, while Fig. 10 shows the relative intensity distribution for different photon energies.

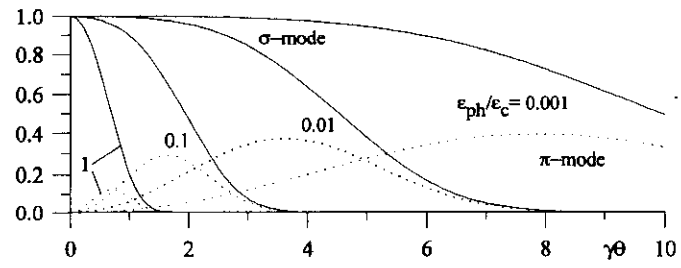

Figure 10: Relative magnitude of $\sigma-$(solid) and $\pi-$mode (dash) radiation

6.5 Statistical Parameters of Synchrotron Radiation

Electron beam parameters like emittances and energy spread are defined by synchrotron radiation characteristics. These equilibrium particle beam parameters depend on some statistical quantities of photon emission.

From the photon spectrum we derive an average photon energy of

$$\langle \varepsilon \rangle = \frac{8}{15\sqrt{3}}\,\varepsilon_c\,. \tag{38}$$

The effect of emission of a photon on the particle trajectory depends on $\langle \varepsilon^2 \rangle$ for which we get

$$\langle \varepsilon^2 \rangle = \frac{11}{27}\,\varepsilon_c^2\,, \tag{39}$$

Finally, the total photon flux can be expressed by

$$\dot{N}_{\rm ph} = \frac{15\sqrt{3}}{8}\,\frac{P_\gamma}{\varepsilon_c}\,. \tag{40}$$

We use these results to determine the equilibrium beam emittance and energy spread.

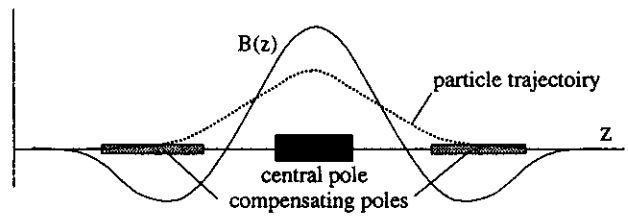

Figure 11: Magnetic field distribution along the beam path for a wave length shifter

7 Insertion Device Radiation

Deflection of a highly relativistic particle beam causes the emission of a broad spectrum of synchrotron radiation as discussed earlier. The width of the spectrum is characterized by the critical photon energy and depends only on the particle energy and the radius of the bending magnet. Generally the radiation is produced in the bending magnets of a storage ring, where a high beam current is stored with a long beam lifetime of several hours. However, in order to adjust to special experimental needs other magnetic devices are being used as well to produce synchrotron radiation. We call such devices *insertion devices*since they do not contribute to the overall deflection of the particle beam in the circular accelerator. Their effect is localized and the overall deflection in an insertion device is zero.

7.1 Wave Length Shifter

To meet the need for harder x-ray radiation in lower energy storage rings it is customary to install in a magnet free section of the ring a *wave length shifter*. Such a device consists of three ordinary dipole magnets with a high field central magnet and two lower field magnets with opposite field direction on either side to compensate the beam deflection by the central pole. As an alternative all three poles may be of the same strength but the side poles are only half as long as the central pole as shown in Fig. 11. Whatever is used, the total deflection angle must be zero or $\int_{\mathrm{WLshifter}} B_y \mathrm{d}s = 0$. The particle beam traversing this wave length shifter is deflected up and down or left and right in such a way that no net deflection remains.

The condition for the longitudinal distribution of the magnetic field in case

of a horizontally deflecting wave length shifter is

$$\int_{-\infty}^{+\infty} B_y(y=0,z)\mathrm{d}z \;=\; 0\,. \tag{41}$$

A wavelength shifter with such field properties is neutral on the geometry of the particle beam path and therefore can be made in principle as strong as necessary or technically feasible. In most cases such wave length shifters are constructed as superconducting magnets with high fields in the central pole which serves as the radiation source at maximum critical photon energy for the given particle beam energy. The fields of the side poles serves mainly to compensate the beam deflection in the central pole.

Some limitations apply for such devices as well as for any other insertion devices. The end fields of magnets can introduce particle focusing and nonlinear field components may introduce aberrations and instability. The radiation characteristics are similar to that of a bending magnet of equal field strength. Specifically we note the broad photon spectrum which extends up to photon energies as determined by the field of the insertion device.

7.2 Undulator Radiation

In contrast to the broadband radiation from bending magnets and wavelength shifters we may generate quasi-monochromatic radiation from periodic oscillatory motion of the electron beam in an undulator magnet. Here, the beam travels in the general direction toward the observer while executing transverse oscillations under the influence of the magnetic Lorentz force. Instead of the short single pulse of bending magnet radiation we observe now radiation over a number of oscillations.

7.2.1 Elementary Processes due to Periodic Motion

The periodic transverse motion is effected by periodic transverse acceleration causing the emission of electromagnetic fields. Radiation is emitted in the electron system similar to that from a radio antenna. There is no radiation along the antenna (acceleration) and maximum intensity is emitted orthogonal to the acceleration. The radiation intensity scales like $I \propto \sin^2\Theta$ and Θ is the angle of radiation emission with respect to the direction of acceleration. Plotting the quantity $\sin^2\Theta$ defines the *radiation lobe* which has in the electron system of reference the form of a doughnut as shown in Fig. 12. The length of the vector from the coordinate origin to the surface of the radiation lobe is proportional to the radiation intensity in that direction.

Of course, transforming this into the laboratory system we find the radiation to be well collimated along the z-axis.

For very weak and perfectly sinusoidal magnetic fields the particle follows a sinusoidal trajectory with similar periodic acceleration. The undulator field strength is measured by the K-parameter defined by $K = \gamma\vartheta$, where ϑ is the

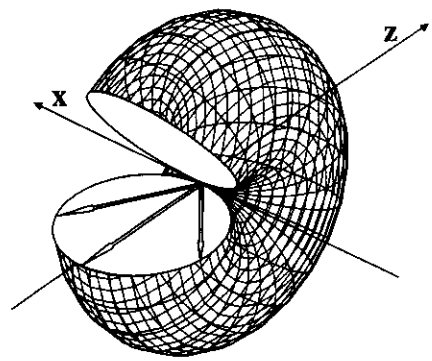

Figure 12: Radiation lobes in the reference system of the electron. Acceleration is along the x-axis.

maximum deflection angle of the particle trajectory from the z-axis as will be discussed later. A weak undulator magnet is then defined by $K < 1$.

Ahead of the undulator the electron and its associated electric field travel with uniform velocity. Upon entering the undulator the electron suddenly starts performing transverse oscillations generating periodic perturbations on the electric field lines. These perturbations travel away from the electron at the speed of light and are recognized by an observer as radiation. The periodic electric field perturbations resemble exactly the motion of the electron as a perfectly sinusoidal perturbation oscillating with the same frequency as the oscillating acceleration. The radiation intensity is proportional to the transverse component of the perturbation (E-field) as seen by the observer and varies with the observation angle.

For N oscillations in the undulator we get N oscillations of the electromagnetic field and after Fourier analysis we find all radiation to be concentrated within al band width of $1/N$ at the frequency of the periodic motion called the *fundamental undulator frequency*. In this weak field case the transverse motion is nonrelativistic. In another equally valid view the static and periodic magnetic undulator field appears to the electron as a Lorentz contracted electromagnetic field or as monochromatic photons of wavelength $\lambda^* = \lambda_p/\gamma$. The emission of photons can therefore be described as Thompson scattering of photons by free electrons resulting in monochromatic radiation in the direction of the particle path.

As the magnetic field is increased and $K > 1$ the transverse motion becomes more and more relativistic. As a consequence, the monochromatic sinusoidal

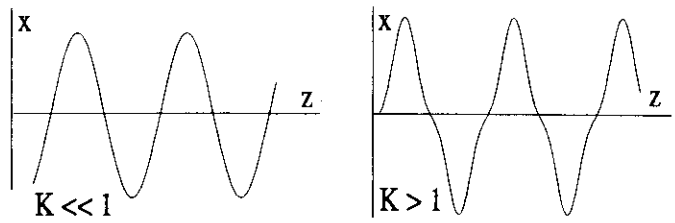

Figure 13: Harmonic generation in strong undulators

motion becomes perturbed by relativistic effects as shown in Fig. 13. Specifically, the perturbation is symmetric about the fundamental sinusoid and generates therefore only odd harmonics. The relativistic perturbations occurs when the particles travel at maximum transverse velocity which happens twice per period. Since this perturbation does not depend on the direction of motion we get a symmetric perturbation of the sinusoidal motion generating only odd harmonics. The radiation now also exhibits in addition to the fundamental frequency increasingly more and more odd harmonics. Undulator radiation therefore can be described by a line spectrum including only odd harmonics of a fundamental frequency.

Upon closer inspection of the particle dynamics with respect to the electric field of the electron we note another perturbation of the trajectory. In the laboratory system the particle performs a periodic transverse motion. With respect to a uniformly traveling reference system, however, we note also a periodic longitudinal motion because the z-component of the particle velocity, v_z, oscillates periodically. A useful reference system would travel, for example, with the average drift velocity of the particle along the z-axis. With respect to this system the electron travels faster while in the vicinity of the crest and valley of the oscillation and slower in between. This leads to a figure-of-8 motion as shown in Fig. 14. Now we have two oscillatory motions, one with transverse acceleration $a_\perp$ and one with longitudinal acceleration $a_\parallel$ at twice the frequency of $a_\perp$. The longitudinal acceleration causes radiation at twice the fundamental frequency and for higher fields at more and more even harmonics.

We have now a line spectrum at all harmonics of the fundamental radiation. Yet, the character of even and odd harmonics are very different. The radiation due to transverse acceleration is emitted mostly along the z-axis while the longitudinal acceleration causes radiation normal with respect to the z^*-axis in the electron system or at an angle of $1/\gamma$ in the laboratory system. Forward radiation through a pin hole along the z-axis includes therefore only odd harmonics while even harmonics appear only in larger apertures. This kind of radiation with one or few harmonics is called *undulator radiation*in contrast with wig-

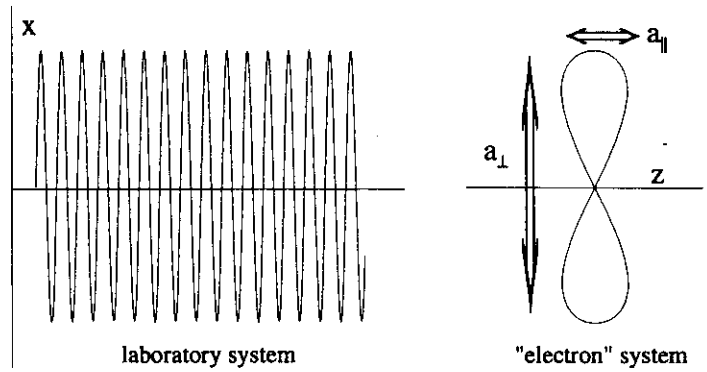

Figure 14: Periodic motion in an undulator magnet seen from the laboratory system and from a system moving with the average drift velocity of the particle.

gler radiation which consists of very many overlapping harmonics forming a broadband synchrotron radiation spectrum as discussed later in these lectures..

7.2.2 Beam Dynamics in an Undulator

The radiation characteristics a greatly determined by the actual path the electrons follow through the undulator magnet. We define therefore first the magnetic field and derive from that the equation of motion.

Undulator field To evaluate more quantitatively the physics of undulator radiation we assume the magnetic field to be represented by a sinusoidal variation, $B_y = B_0 \cos(k_p z)$ along the z- axis

$$\begin{aligned} B_x &= 0\,, \\ B_y &= B_0 \cosh k_p y \cos k_p z\,, \\ B_z &= -B_0 \sinh k_p y \sin k_p z\,, \end{aligned} \tag{42}$$

where $\lambda_p = 2\pi/k_p$ is the period length. The particle trajectory and with it the radiation characteristics are defined by the components of this field.

Particle equation of motion The equation of motion for an electron in the undulator field can be derived from

$$\frac{\mathbf{n}}{\rho} = \frac{e}{m\gamma v_0^2}\,[\mathbf{v} \times \mathbf{B}]\,. \tag{43}$$

After two integrations we get the solutions in component form

$$x(t) = \frac{K}{\gamma k_\mathrm{p}} \cos\left(k_\mathrm{p} \bar{\beta} c t\right) , \tag{44}$$

$$z(t) = \bar{\beta} c t + \frac{K^2}{8 k_\mathrm{p} \gamma^2} \sin(2 k_\mathrm{p} \bar{\beta} c t) , \tag{45}$$

where we define the average drift velocity by

$$\bar{\beta} = \beta \left(1 - \frac{K^2}{4\gamma^2}\right) . \tag{46}$$

The maximum oscillation amplitude a is

$$a = \frac{K}{\gamma k_\mathrm{p}} \tag{47}$$

and the deflection angle of the trajectory ϑ from the axis is

$$\vartheta = \frac{B_\mathrm{o}}{B\rho} \frac{\lambda_\mathrm{p}}{2\pi} , \tag{48}$$

and strength parameter

$$K = \frac{e B_\mathrm{o}}{\beta m c k_\mathrm{p}} = \gamma \vartheta = 93.4\, B\, \lambda_\mathrm{p} . \tag{49}$$

7.2.3 Radiation Power

The total energy loss of an electron passing through a N-period wiggler or undulator magnet of length $L_\mathrm{u} = N\, \lambda_\mathrm{p}$ can be obtained by performing the integration (14) through the whole undulator magnet. With some parameters substitutions we get for the energy loss of an electron passing through an undulator

$$\Delta E_\mathrm{rad} = \tfrac{1}{3}\, r_\mathrm{c}\, m c^2\, \gamma^2\, K^2\, k_\mathrm{p}^2\, L_\mathrm{u} \tag{50}$$

or in practical units

$$\Delta E_\mathrm{rad}(\mathrm{eV}) = 0.07257\, \frac{E^2\, K^2}{\lambda_\mathrm{p}^2}\, L_\mathrm{u} . \tag{51}$$

A circulating beam current I, finally, generates a total photon beam power of

$$P = \frac{4\pi^2\, r_\mathrm{c}}{3\, e\, m c^2}\, \frac{E^2\, K^2\, N\, I}{\lambda_\mathrm{p}} \tag{52}$$

or

$$P(\mathrm{W}) = 0.07257\, \frac{E^2\, K^2\, N\, I}{\lambda_\mathrm{p}} , \tag{53}$$

7.2.4 Fundamental Undulator Wavelength

Viewed from the laboratory system the radiation is Doppler shifted and applying (8) we get the wave length of the backscattered photons

$$\lambda_\gamma = \frac{\lambda_p}{\gamma^2 (1 + \beta n_z^*)} . \tag{54}$$

Viewing the radiation in the forward direction we use the third equation (9) and get with $\Theta \ll 1$, $n_z = \cos\Theta^* \approx 1 - \frac{1}{2}\Theta^{*2}$ and $\beta \approx 1$

$$1 + \beta n_z^* = \frac{\beta + n_z^*}{n_z} \approx \frac{2 - \frac{1}{2}\Theta^{*2}}{n_z} . \tag{55}$$

Since $n_z \approx 1$ the wavelength of the emitted radiation is

$$\lambda_\gamma = \frac{\lambda_p}{\gamma^2} \frac{1}{2 - \frac{1}{2}\Theta^{*2}} \approx \frac{\lambda_p}{2\gamma^2}(1 + \tfrac{1}{2}\Theta^{*2}). \tag{56}$$

With (10) the angle Θ^* of the particle trajectory with respect to the direction of observation we get the corresponding angle in the laboratory system, $\Theta^* = 2\gamma\Theta$. The observation angle Θ has two components, one is the observation angle with respect to the axis and the other originates from the deflection of the beam path in the undulator generating a modulation of the actual observation angle. We set therefore $\Theta = \Psi + K/\gamma \sin k_p z$ and the average of the square is then just $\Theta^2 = \Psi^2 + \frac{1}{2}K^2/\gamma^2$ since the cross term averages out. This result is correct for a *flat undulator*. For a *helical undulator* the electron trajectory spirals at a constant angle around the axis and the factor 1/2 is omitted. Here, we use only a flat undulator. we split the observation angle Ψ into a horizontal angle ψ and a vertical component θ and get with $\Psi^2 = \psi^2 + \theta^2$ for the wavelength of undulator radiation

$$\lambda_i = \frac{\lambda_p}{2i\gamma^2}[1 + \tfrac{1}{2}K^2 + \gamma^2(\theta^2 + \psi^2)] , \tag{57}$$

where we have included the fact that undulator radiation can be emitted also at harmonics i of the *fundamental wavelength* at $i = 1$ which is the only wavelength emitted for very weak fields $K \ll 1$. As the undulator parameter increases, however, the oscillatory motion of the particle in the undulator deviates from a pure sinusoidal oscillation. For $K > 1$ the transverse motion becomes relativistic, causing a deformation of the sinusoidal motion and the creation of higher harmonics as discussed earlier. These harmonics appear at integral multiples of the fundamental radiation energy. Only odd harmonics are emitted in the forward direction, $\theta \approx 0$, while the even harmonics are emitted into finite angles with respect to the axis.

The wavelength for $\theta = \psi = 0$ is in practical units for electrons

$$\lambda_i(\text{Å}) = 1305.6 \frac{\lambda_p}{i E^2}(1 + \tfrac{1}{2}K^2) , \tag{58}$$

and the corresponding photon energy

$$\varepsilon_i(\mathrm{eV}) = 9.4963 \cdot \frac{i\,E^2}{\lambda_\mathrm{p}(1+\frac{1}{2}K^2)}\,. \tag{59}$$

7.2.5 Band Width

The electron motion through an undulator with N periods includes N oscillations and so does the radiation. From Fourier theory we know that such a pulse has a line width of

$$\frac{\Delta\lambda}{\lambda} = \frac{1}{N}\,. \tag{60}$$

The electromagnetic field emitted from an electron traveling through an undulator has oscillatory character for a limited time and represents therefore narrow band radiation in contrast to bending magnet radiation which appears to the observer only as a very short pulse.

7.2.6 Photon Beam Collimation

Due to the coherent superposition of radiation from the same electron but from many undulator periods we observe an enhanced collimation of undulator radiation beyond that of ordinary synchrotron radiation. The radiation opening angle is

$$\sigma_\theta = \frac{1}{\gamma}\sqrt{\frac{1+\frac{1}{2}K^2}{2iN_\mathrm{p}}} \tag{61}$$

The collimation increases with the square root of the number of undulator periods and the harmonic number. In Fig. 15 a picture of undulator radiation tuned to visible light is shown and gives some impression of collimation. The undulator deflection occurs in the horizontal plane and in the color version of this picture we observe blue light in the center and increasing red shift as radiation is observed at some angle.

7.2.7 Spatial and Spectral Photon Flux

The particular path of an electron traveling through an undulator determines the spectral and spatial photon flux. Considering a circulating beam current I this flux at the harmonic i and for both σ- and π-mode polarization is given by

$$\frac{\mathrm{d}\dot{N}_\mathrm{ph}(\omega)}{\mathrm{d}\Omega} = \alpha\,\gamma^2\,N_\mathrm{p}^2\frac{\Delta\omega}{\omega}\frac{I}{e} \times \sum_{i=1}^{\infty} i^2\,\mathrm{Sinc}\,(F_\sigma^2 + F_\pi^2)\,. \tag{62}$$

The frequency ω_1 is the fundamental undulator frequency,

$$\mathrm{Sinc} = \left(\frac{\sin\pi N_\mathrm{p}\Delta\omega_i/\omega_1}{\pi N_\mathrm{p}\Delta\omega_i/\omega_1}\right)^2\,, \tag{63}$$

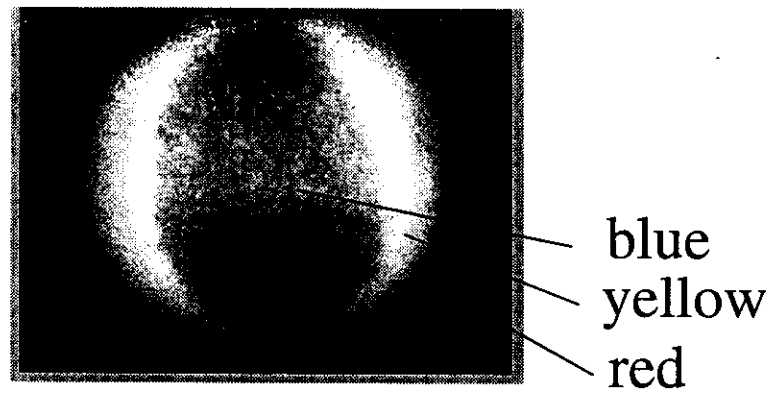

Figure 15: Black and white rendition of undulator radiation tuned to visible light

and

$$F_\sigma = \frac{2\gamma\theta\Sigma_1\cos\varphi - K\,\Sigma_2}{1+\frac{1}{2}K^2+\gamma^2\theta^2}\,, \tag{64}$$

$$F_\pi = \frac{2\gamma\theta\Sigma_1\sin\varphi}{1+\frac{1}{2}K^2+\gamma^2\theta^2}\,, \tag{65}$$

where $\Delta\omega_i = \omega - \omega_i$, and

$$\Sigma_{1,i} = \sum_{\substack{m=\\-\infty}}^{\infty} J_{-m}(u)J_{i-2m}(v)\,,$$

$$\Sigma_{2,i} = \sum_{\substack{m=\\-\infty}}^{\infty} J_{-m}(u)[J_{i-2m-1}(v)+J_{i-2m+1}(v)]$$

$$u = \frac{\omega}{\omega_1}\frac{\bar\beta\,K^2}{4(1+\frac{1}{2}K^2+\gamma^2\theta^2)}\,,$$

$$v = \frac{\omega}{\omega_1}\frac{2\bar\beta\,K^2\gamma\theta\,\cos\varphi}{1+\frac{1}{2}K^2+\gamma^2\theta^2}\,.$$

Here the angle θ is taken with respect to the beam axis and φ is the azimuthal angle counted counterclockwise while viewing the source with $\varphi = 0$ in the deflection plane. This is the general solution describing undulator radiation without approximation. The *Sinc*-function actually describes the line spectrum while all other terms vary slowly with photon frequency.

7.2.8 Pinhole Radiation

For practical applications we concentrate mainly on the forward radiation emitted at $\theta = 0$ and at the maximum of the harmonic frequencies where $\Delta\omega_i = 0$. This is the radiation generally used by experimenters while the radiation between harmonics is low in intensity and of no practical interest. This forward radiation is selected commonly by installation of a pinhole with a small aperture to transmit only forward radiation or *pinhole radiation*. With these assumptions the spatial and spectral photon flux distribution in the i-th harmonic is

$$\left.\frac{\mathrm{d}\dot{N}_{\mathrm{ph}}(\omega)}{\mathrm{d}\Omega}\right|_i = \alpha\gamma^2 N_{\mathrm{p}}^2 \frac{\Delta\omega}{\omega}\frac{I}{e}\frac{i^2\,K^2\,[JJ]^2}{\left(1+\frac{1}{2}K^2\right)^2}$$

$$= 1.7466\cdot 10^{23}\,E^2(\mathrm{GeV}^2)I(\mathrm{A})N_{\mathrm{p}}^2\frac{\Delta\omega}{\omega}\,f_i(K)\,, \qquad (66)$$

with

$$[JJ] = \left[J_{\frac{i-1}{2}}(x) - J_{\frac{i+1}{2}}(x)\right], \qquad (67)$$

and $x = \frac{iK^2}{4+2K^2}$. The function $f_i(K) = \frac{i^2\,K^2\,[JJ]^2}{\left(1+\frac{1}{2}K^2\right)^2}$ is graphed in Fig. 16 and tabulated for practical application in table 1.

Table 1: Tabulation of function $f_i(K)$

K	f_1	f_3	f_5	f_7	f_9	f_{11}
0.1	0.010	0.000	0.000	0.000	0.000	0.000
0.2	0.038	0.000	0.000	0.000	0.000	0.000
0.4	0.132	0.004	0.000	0.000	0.000	0.000
0.6	0.238	0.027	0.002	0.000	0.000	0.000
0.8	0.322	0.087	0.015	0.002	0.000	0.000
1.0	0.368	0.179	0.055	0.015	0.004	0.001
1.2	0.381	0.276	0.128	0.051	0.019	0.007
1.4	0.371	0.354	0.219	0.118	0.059	0.028
1.8	0.320	0.423	0.371	0.286	0.206	0.142
2.0	0.290	0.423	0.413	0.354	0.285	0.220
5.0	0.071	0.139	0.188	0.228	0.261	0.290
10.0	0.019	0.037	0.051	0.068	0.075	0.085
20.0	0.005	0.010	0.013	0.016	0.019	0.022

Undulator radiation is extremely collimated and therefore the *angle integrated* spectral flux is of interest. Performing this integration the total spectral pinhole photon flux in the harmonic i is

$$\dot{N}_{\mathrm{ph}}(\omega)|_i = \pi\alpha N_{\mathrm{p}}\frac{\Delta\omega}{\omega}\frac{I}{e}\frac{i\,K^2\,[JJ]^2}{1+\frac{1}{2}K^2} = 1.431\,10^{17}\,I(\mathrm{A})\,N_{\mathrm{p}}\frac{\Delta\omega}{\omega}\,g_i(K)\,, \qquad (68)$$

where $g_i(K) = f_i(K)\frac{1+\frac{1}{2}K^2}{i} = \frac{i\,K^2\,[JJ]}{1+\frac{1}{2}K^2}$.

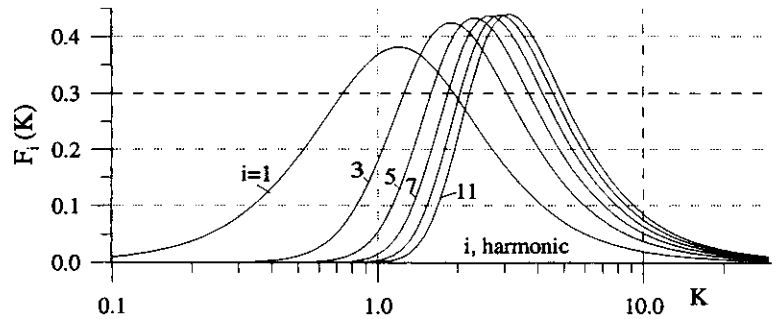

Figure 16: Function $f_i(K) = \frac{i^2 K^2 [JJ]}{(1+\frac{1}{2}K^2)^2}$

Fig.17 shows the measured linespectrum from an undulator at different strengths. For $K \ll 1$ we note only one line in the radiation spectrum with more appearing as K is increased. As the undulator strength approaches and exceeds unity the transverse motion of the electrons becomes relativistic distorting the purely sinusoidal motion. Higher harmonics of the oscillatory motion give cause for the appearance of higher harmonics in the radiation spectrum. As the undulator strength is further increased more and more harmonics appear, each of them growing wider and finally merging into the well-known broad spectrum of a bending or wiggler magnet.

The concentration of all radiation into one or few lines is very desirable for many experiments utilizing monochromatic photon beams since radiation is produced only in the vicinity of the desired wavelength at high brightness. Radiation at other wavelengths creating undesired heating effects on optical elements and samples is greatly reduced.

7.2.9 Tunability of Undulator Radiation

To maximize the photon flux it is desirable to construct an undulator with many periods N_p which is difficult to do for electromagnetically excited poles. Generally, undulators are constructed of permanent magnet material which allows designs with a period length of only a few cm. On the other hand, however, the user would like to vary the photon frequency. The only way to vary the field seen by the electron beam is to change the gap between magnet poles. this will change the magnetic field and thereby the K-parameter and radiation wavelength.

The magnetic field strength between permanent magnet poles depends on the distance between those poles or on the gap height g. By varying mechanically the gap height of a permanent magnet wiggler the magnetic field strength can be varied as well. The field strength also depends on the period length and on the design and magnet materials used. For a wiggler magnet constructed as

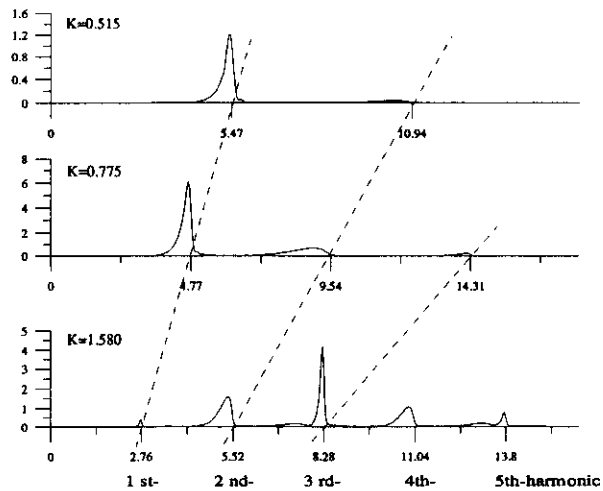

Figure 17: Measured radiation spectrum from an undulator for different strength parameters K. Note, that the intensity at low photon energies are reduced by absorption in a Be-window.

a hybrid magnet with Vanadium Permendur poles the field strength along the midplane axis scales approximately like

$$B_y(\text{Tesla}) \approx 3.33\text{e}^{-\frac{g}{\lambda_p}\left(5.47-1.8\frac{g}{\lambda_p}\right)} \quad \text{for} \quad g \geq \lambda_p\,, \tag{69}$$

where g is the gap aperture between magnet poles. This dependency is also shown in Fig. 18 and we note immediately that the field strength drops off dramatically for magnet gaps comparable to the period length. The undulator strength parameter K is then just $K = 0.934 B_y(\text{Tesla})\lambda_p(\text{cm})$.

On the other hand a significant field strength can be obtained for small gap apertures and it is therefore important to design for or find locations for the insertion device in a beam transport line, where the beam dimension normal to the deflection plane is very small. The minimum allowable gap determines the highest value of the undulator strength K. Since the fundamental undulator wavelength depends on this strength like $\lambda_1 \propto (1 + \frac{1}{2}K^2)$ the minimum gap determines the low photon energy limit. Opening the gap reduces K and the fundamental wavelength is reduced. Of course, the intensity also decreases if the K-parameter is reduced too much. The relative intensities for different harmonics and different values of K can be observed from Fig. 16.

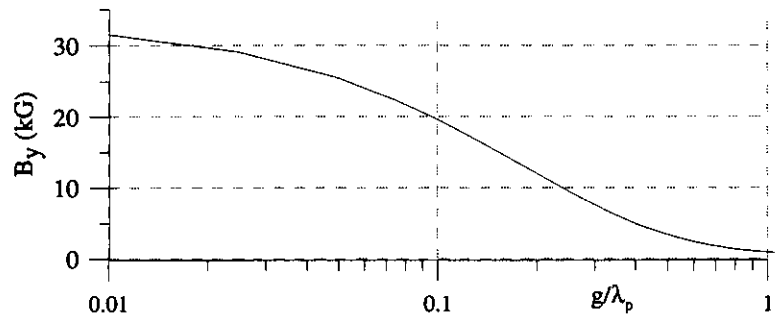

Figure 18: On axis field strength in a Vanadium Permendur hybrid wiggler magnet as a function of gap-aperture

7.3 Wiggler Magnet Radiation

The principle of a wave length shifter is extended in the case of a *wiggler magnet*. Such a magnet consists of a series of equal dipole magnets with alternating magnetic field direction. Again the end poles must be configured to make the total device neutral to the geometry of the particle beam path such that $\int B_y(y=0,z)\,\mathrm{d}z = 0$.

The advantage of using many magnet poles is to increase the photon flux. Each of N magnet poles produces a fan of radiation in the forward direction and the total photon flux is N times larger than that from a single pole. Wiggler magnets may be constructed as electromagnets with strong fields to function both as a wavelength shifter and flux enhancer.

To maximize photon flux wiggler magnets are constructed from permanent magnet materials. This construction technique results in rather short field periods allowing many wiggler poles for a given space in the storage ring lattice.

The longitudinal field distribution assumes the form of an alternating step function for magnet poles which are long compared to the gap aperture. Most wiggler magnets are however optimized to enhance the photon flux which requires many short magnet poles. In this case the magnetic field distribution is sinusoidal with a period length λ_p

$$B_y(x, y=0, z) \;=\; B_\mathrm{o} \sin 2\pi \frac{z}{\lambda_\mathrm{p}}\,. \tag{70}$$

The deflection angle per half pole is

$$\vartheta \;=\; \frac{B_\mathrm{o}}{B\rho} \int_\mathrm{o}^{\lambda_\mathrm{p}/4} \sin 2\pi \frac{z}{\lambda_\mathrm{p}} \mathrm{d}z \;=\; \frac{B_\mathrm{o}}{B\rho} \frac{\lambda_\mathrm{p}}{2\pi}\,, \tag{71}$$

where $B\rho$ is the beam rigidity. Multiplying this with the beam energy γ we

define the wiggler *strength parameter* K

$$K = \gamma\vartheta = 0.934\, B(\text{Tesla})\, \lambda_p(\text{cm}) . \tag{72}$$

This wiggler strength parameter is generally much larger than unity. Conversely, a series of alternating magnet poles is called a wiggler magnet if the strength parameter $K \gg 1$.

Fig. 19 shows the line spectrum as a function of the strength parameter K. For $K < 1$ only few harmonics are obvious while for $K \gg 1$ the line spectrum approaches the continuous synchrotron radiation spectrum of a wiggler or bending magnet.

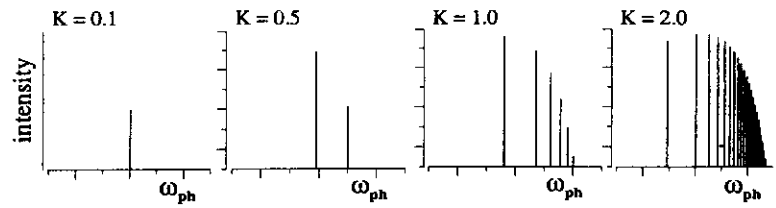

Figure 19: Line spectra of wiggler/undulator radiation for increasing strength parameter K

The critical photon energy of wiggler radiation depends on the observation angle ψ in the deflecting plane because of a varying magnetic field and is given by

$$\varepsilon_c(\psi) = \varepsilon_c(0) \sqrt{1 - \left(\frac{\gamma\psi}{K}\right)^2} . \tag{73}$$

7.4 Laser Backscattering

The principle of Thomson backscattering of the static undulator fields can be expanded to that of photon beams colliding head on with the particle beam. In the electron system of reference the electromagnetic field of this photon beam looks fundamentally no different than the electromagnetic field from the undulator magnet. We may therefore apply similar arguments to determine the wavelength of back scattered photons. The basic difference of both effects is that in the case of back scattered photons the photon beam moves with the velocity of light towards the electron beam and therefore the electron *sees* twice the Lorentz contracted photon frequency and expect therefore a beam of back scattered photons which is twice Doppler shifted. That extra factor of two does not apply for undulator radiation since the undulator field is static and the relative velocity with respect to the electron beam is c. If λ_p is the wavelength of the incident radiation, the wavelength of the backscattered photons is

$$\lambda_\gamma = \frac{\lambda_p}{4\gamma^2} \left(1 + \tfrac{1}{2}\gamma^2\vartheta^2\right), \tag{74}$$

where ϑ is the angle between the direction of observation and the particle beam axis. Scattering for example a high intensity laser beam from high-energy electrons produces a monochromatic beam of hard x-rays which is highly collimated within an angle of $\pm 1/\gamma$. If $\lambda_p = 10\mu$m and the particle energy is 100 MeV the wave length of the backscattered x-rays would be 1.3 Åor the photon energy would be 9.5 keV.

7.4.1 Radiation Intensity

The intensity of the backscattered photons can be calculated in a simple way utilizing the Thomson scattering cross section

$$\sigma_{\text{Th}} = \frac{8\pi}{3} r^2 = 6.65 \times 10^{-25}\,\text{cm}^2 . \tag{75}$$

The total scattering event rate or the number of back scattered photons per unit time is then

$$N_{\text{sc}} = \sigma_{\text{Th}}\, \mathcal{L} , \tag{76}$$

where $\mathcal{L}$ is called the *luminosity*. The value of the luminosity is independent of the nature of the physical reaction and depends only on the intensities and geometrical dimensions of the colliding beams.

The number of backscattered photons or the luminosity can be determined by folding the particle density in one beam with the incident "particles" per unit time of the other beam. Obviously only those parts of the beam cross sections count which overlaps with the cross section of the other beam. For simplicity we assume a gaussian distribution in both beams and assume that both beam cross sections are the same. We further consider the particle beam as the target for the photon beam. With N_e electrons in each bunch of the particle beam within a cross section of $4\pi\sigma_x\sigma_y$ the particle density is $N_e/(4\pi\sigma_x\sigma_y)$.

We consider now for simplicity a photon beam with the same time structure as the electron beam. If this is not the case only that part of the photon beam which actually collides with the particle beam within the collision zone may be considered. For an effective photon flux $\dot{N}_{\text{ph}}$ the luminosity is

$$\mathcal{L} = \frac{N_e \dot{N}_{\text{ph}}}{4\pi\, \sigma_x\, \sigma_y} . \tag{77}$$

The photon flux may be better expressed in terms of laser power in which case we set $\dot{N}_{\text{ph}} = P_{\text{laser}}/\varepsilon_{\text{ph}}$ where ε_{ph} is the laser photon energy. Of course, this luminosity and the rate of backscattered photons occurs only while both the electron beam and the laser beam collide. This is dependent on both the electron bunch structure and the laser pulse structure.

Although the Thomson cross section and therefore the photon yield is very small this technique can be used to produce photon beams with very specific characteristics. For example, letting the electron beam collide with a very short laser pulse can produce an equally short burst of highly collimated x-rays which would not be possible any other known way.

So far, it was assumed that the incident and scattered photon energies are much smaller than the particle energy in which case it was appropriate to use the classical case of Thomson scattering. However, we note that equation (74) diverges in the sense that shorter and shorter wavelength radiation can be produced if only the particle energy is increased more and more. The energy of the backscattered photons, on the other hand, increases quadratically with the particle energy and therefore at some energy the photon energy becomes larger than the particle energy which is unphysical. In case of large photon energies with respect to the particle energy, the Compton corrections must be included.

The Compton cross section is given by

$$\sigma_{\rm C} = \frac{3\sigma_{\rm Th}}{4\,x}\left\{\left(1-\frac{4}{x}-\frac{8}{x^2}\right)\ln(1+x)+\frac{1}{2}+\frac{8}{x^2}-\frac{1}{2(1+x)^2}\right\}, \qquad (78)$$

where $x = \{4\gamma\hbar\omega_{\rm o}/(mc^2)\}\cos^2(\alpha_{\rm o}/2)$, $\gamma = E/(mc^2)$ the particle energy in units of the rest energy $\hbar\omega_{\rm o}$ the incident photon energy and $\alpha_{\rm o}$ the angle between particle motion and photon direction with $\alpha_{\rm o} = 0$ for head on collision. The energy spectrum of the scattered photons is then

$$\frac{{\rm d}\sigma_C}{{\rm d}y} = \frac{3\sigma_{\rm Th}}{4\,x}\left\{1-y+\frac{1}{1-y}-\frac{4\,y}{x\,(1+y)}+\frac{4y^2}{x^2\,(1-y)^2}\right\}, \qquad (79)$$

where $y = \hbar\omega/E < y_{\rm max}$ is the scattered photon energy in units of the particle energy and $y_{\rm max} = x/(1+x)$ is the maximum energy of the scattered photons.

8 Brightness and Coherence

In this section we will discuss the physics of spontaneous coherent synchrotron radiation while distinguishing two kinds of coherence in synchrotron radiation, the *temporal coherence* and the *spatial coherence*. Temporal coherence occurs when all radiating electrons are located within a short bunch of the order of the wavelength of the radiation. In this case the radiation from all electrons is emitted with the same phase. For spatial coherence the electrons may be contained in a long bunch but the transverse beam emittance must be smaller than the radiation wavelength. In either case there is a smooth transition from incoherent radiation to coherent radiation as the bunch length or transverse emittance is gradually reduced.

8.1 Spatial Coherence

Synchrotron radiation is emitted from a rather small area equal to the cross section of the electron beam. In the extreme and depending on the photon wave length the radiation may be spatially coherent because the beam cross section in phase space is smaller than the wave length. This possibility to create spatially coherent radiation is important for many experiments specifically for holography and we will discuss in more detail the conditions for the particle beam to emit such radiation.

Reducing the particle beam cross section in phase space by diminishing the particle beam emittance reduces also the source size of the photon beam. This process of reducing the beam emittance is, however, effective only to some point. Further reduction of the particle beam emittance would have no effect on the photon beam emittance because of *diffraction*effects. A point like photon source appears in an optical instrument as a disk with concentric illuminated rings. For synchrotron radiation sources it is of great interest to maximize the photon beam *brightness* which is the photon density in phase space. On the other hand designing a lattice for a very small beam emittance can causes beam stability problems. It is therefore prudent not to push the particle beam emittance to values much less than the diffraction limited photon beam emittance. In the following we will therefore define diffraction limited photon beam emittance as a guide for low emittance lattice design.

8.2 Diffraction

For highly collimated synchrotron radiation it is appropriate to assume Fraunhofer diffraction. Radiation from an extended light source appears diffracted in the image plane with a radiation pattern which is characteristic for the particular source size and radiation distribution as well as for the geometry of the apertures involved. For simplicity, we will use the case of a round aperture being the boundaries of the beam itself although in most cases the beam cross section is more elliptical. In spite of this simplification, however, we will obtain all basic physical properties of diffraction which are of interest to us.

We consider a circular light source with diameter $2a$. The radiation field at point P (Fig. 20) in the image plane is then determined by the *Fraunhofer diffraction integral*

$$U(P) \;=\; C \int_0^a \int_0^{2\pi} \mathrm{e}^{-\mathrm{i}k\,\rho\,w\cos(\Theta-\psi)}\mathrm{d}\Theta\rho\mathrm{d}\rho\,. \tag{80}$$

With $\alpha = \Theta - \psi$ and the definition of the zeroth order Bessel's function

$$J_0(x) \;=\; \frac{1}{2\pi}\int_0^{2\pi} \mathrm{e}^{-\mathrm{i}\,x\cos\alpha}\mathrm{d}\alpha\,, \tag{81}$$

and (80) can be expressed by the integral

$$U(P) \;=\; 2\pi\,C \int_0^a J_0(k\,\rho\,w)\rho\mathrm{d}\rho\,, \tag{82}$$

which can be solved analytically as well with the identity

$$\int_0^x y\,J_0(y)\,\mathrm{d}y \;=\; x\,J_1(x)\,. \tag{83}$$

The radiation intensity is proportional to the square of the radiation field and we get finally for the radiation intensity in the image plane at point P

$$I(P) \;=\; I_0\frac{4J_1^2(k\,a\,w)}{(k\,a\,w)^2}\,, \tag{84}$$

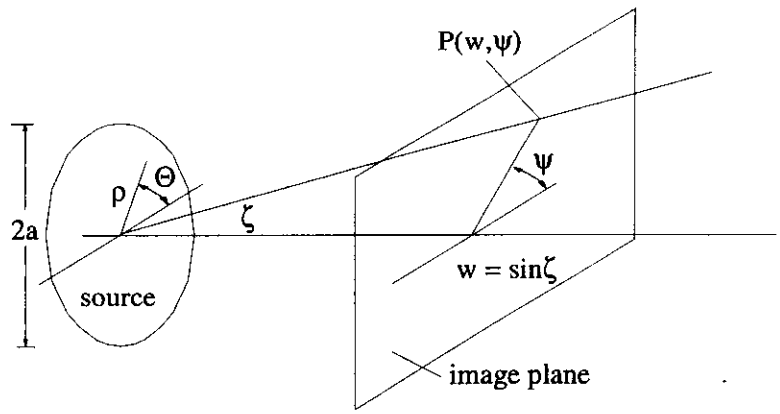

Figure 20: Diffraction geometry

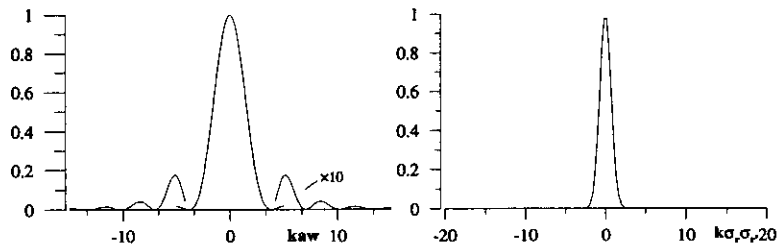

Figure 21: Fraunhofer diffraction for a circular light source illuminated uniformly (left) and with a gaussian illumination (right)

where $I(P) = |U(P)|^2$ and $I_o = I(w = 0)$ is the radiation intensity at the image center. This result has been derived first by Airy. The radiation intensity from a light source of small circular cross section is distributed in the image plane due to diffraction into a central circle and concentric rings illuminated as shown on the left side of Fig. 21.

So far we have assumed that the distribution of light emission from the source is uniform which is generally not correct for a particle beam. A Gaussian distribution is more realistic resembling the distribution of independently radiating particles. We must be careful in the choice of the scaling parameter. The relevant quantity for the Fraunhofer integral is not the actual particle beam size at the source point but rather the apparent beam size and distribution. By folding the particle density distribution with the argument of the Fraunhofer diffraction integral we get the radiation field from a round, Gaussian particle

beam,

$$U_g(P) = \text{const} \int_o^\infty e^{-\frac{\rho^2}{2\sigma_r^2}} J_o(k\rho\sigma_{r'})\rho d\rho, \tag{85}$$

where σ_r is the apparent standard source radius and $w = \sigma_{r'}$ the standard value of the radiation divergence. Introducing the variable $x = \rho/\sqrt{2}\sigma_r$ and replacing

$$k\rho\sigma_{r'} = 2x\sqrt{\frac{k^2\sigma_r^2\sigma_{r'}^2}{2}} = 2x\sqrt{z} \tag{86}$$

we get from (85)

$$U_g(P) = \text{const} \int_o^\infty e^{-x^2} x J_o(2x\sqrt{z}) dx \tag{87}$$

and after integration

$$U_g(P) = \text{const} \exp[-\tfrac{1}{2}(k\sigma_r\sigma_{r'})^2]. \tag{88}$$

The diffraction pattern from a Gaussian light source does not exhibit the ring structure of a uniformly illuminated source as is shown in in the graph on the right side of Fig. 21. The radiation field assumes rather the form of a gaussian distribution with a standard width of

$$k\sigma_r\sigma_{r'} = 1. \tag{89}$$

8.2.1 Diffraction Limited Emittance

Similar to the particle beam characterization through its emittance we may do the same for the photon beam and doing so for the horizontal or vertical plane we have with $\sigma_{x,y} = \sigma_r/\sqrt{2}$ and $\sigma_{x',y'} = \sigma_{r'}/\sqrt{2}$ the photon beam emittance

$$\epsilon_{ph,x,y} = \frac{1}{2}\sigma_r\sigma_{r'} = \frac{\lambda}{4\pi}. \tag{90}$$

This is the *diffraction limited photon emittance* and reducing the electron beam emittance below this value would not lead to an additional reduction in the photon beam emittance. To produce a spatially coherent or diffraction limited radiation source the particle beam emittance must be less than the diffraction limited photon emittance

$$\epsilon_{x,y} < \frac{\lambda}{4\pi}. \tag{91}$$

Obviously, this condition is easier to achieve for long wavelengths. For a spatially coherent radiation source for visible light, for example, the electron beam emittance must be smaller than about $5 \times 10^{-8}\,\pi$ rad-m.

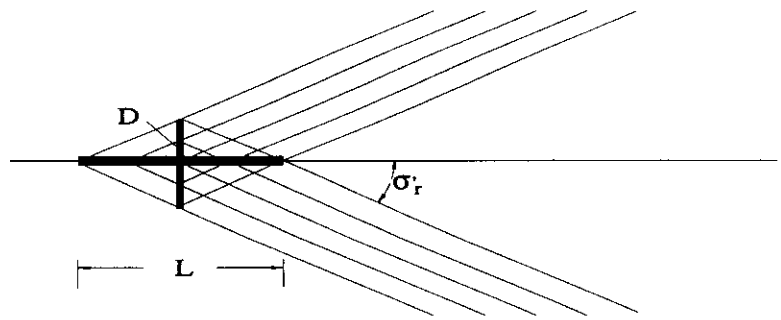

Figure 22: Apparent photon beam source size

8.2.2 Minimum Photon Beam Size and Divergence

After having determined the diffraction limited photon emittance we may also determine the apparent photon beam size and divergence. The photon source extends over some finite length L along the particle path which could be either the path length required for a deflection angle of $2/\gamma$ or a much longer length in the case of an undulator radiation source to be discussed in the next section. With $\sigma_{r'}$ the diffraction limited beam divergence the photons seem to come from a disc with diameter (Fig. 22)

$$D = \sigma_{r'} L \,. \tag{92}$$

On the other hand we know from diffraction theory the correlation

$$D \sin \sigma_{r'} \approx D\sigma_{r'} = \lambda \tag{93}$$

and eliminating D from both equations gives the diffraction limited photon beam divergence

$$\sigma_{r'} = \sqrt{\frac{\lambda}{L}} \,. \tag{94}$$

With this we get finally from (90) also the diffraction limited source size

$$\sigma_r = \frac{\sqrt{\lambda L}}{2\pi} \,. \tag{95}$$

The apparent diffraction limited, radial photon beam size and divergence depend both on the photon wavelength of interest and the length of the source.

9 Photon Beam Brightness

The density of photons in 6-dim phase space is called the photon beam brightness defined for a Gaussian beam sizes and divergence by

$$\mathcal{B} = \frac{N_{\rm ph}}{4\pi^2 \sigma_{{\rm t},x}\sigma_{{\rm t},x'}\sigma_{{\rm t},y}\sigma_{{\rm t},y'}({\rm d}\omega/\omega)}\,, \tag{96}$$

where $N_{\rm ph}$ is the photon flux and $\sigma_{{\rm t},u}$ are the effective photon source sizes. The diffraction limited brightness is with $\sigma_{x,y} = \sigma_r/\sqrt{2}$, etc.

$$\mathcal{B}_{\rm max} = \frac{4\,N_{\rm ph}}{\lambda^2 \frac{{\rm d}\omega}{\omega}}\,. \tag{97}$$

For a real particle beam, the diffraction limited photon emittance becomes diluted due to beam and source appearance effects. Geometrical considerations increase apparent source size from the ideal source size in the middle of the undulator. The diluted beam parameters are given by

$$\begin{aligned}
\sigma^2_{{\rm t},x} &= \tfrac{1}{2}\sigma^2_r + \sigma^2_{{\rm bo},x} + a^2 + \tfrac{1}{12}\sigma^2_{{\rm bo},x'}L^2 + \tfrac{1}{36}\psi^2 L^2\,, \\
\sigma^2_{{\rm t},x'} &= \tfrac{1}{2}\sigma^2_{r'} + \sigma^2_{{\rm bo},x'} && (98)\\
\sigma^2_{{\rm t},y} &= \tfrac{1}{2}\sigma^2_r + \sigma^2_{{\rm bo},y} + \tfrac{1}{12}\sigma^2_{{\rm bo},y'}L^2 + \tfrac{1}{36}\theta^2 L^2\,, && (99)\\
\sigma^2_{{\rm t},y'} &= \tfrac{1}{2}\sigma^2_{r'} + \sigma^2_{{\rm bo},y'}\,. && (100)
\end{aligned}$$

Several effects contribute to this dilution. The photon source width is widened by the finite path oscillation amplitude $a = \lambda_{\rm p}K/(2\pi\gamma)$ in the deflecting plane of the undulator . Variation of the beam sizes along the undulator generates another diluting effect covered by the $1/12$...-terms. Finally, oblique observation at a finite horizontal ψ or vertical angle θ with respect to the optical axis generates the $(1/36$..-terms).

9.1 Matching

In case of a finite particle beam emittance the photon beam brightness is reduced. The amount of reduction, however, depends on the *matching to the photon beam*. The photon beam size and divergence are the result of folding diffraction with electron beam size and divergence. In cases where the electron beam emittance becomes comparable to the diffraction limited emittance the photon beam brightness can be greatly affected by the particular matching condition at the source point .

As an example, the left side of Fig. 23 shows a situation of poor matching in the 2- dimensional $x - x'$-phase space. In this case the electron beam width is very large compared to the diffraction limited source size and its divergence is very small compared to the diffraction limit. The photon beam distribution in phase space is the folding of both electron beam parameters and diffraction limits and is much larger than either one of its components. The photon beam

width is dominated by the electron beam width and the photon beam divergence is dominated by the diffraction limit. Consequently, the effective photon density in phase space and photon beam brightness is reduced.

To improve the situation one would focus the electron beam more to make a smaller beam width at the source point at the expense of increasing the electron beam divergence. the reduction of the electron beam width increase directly the brightness while the related increase of the electron beam divergence is ineffective because the diffraction limits the dominant term. Applying more focusing may give a situation shown on the right side of Fig. 23 where the folded photon phase space distribution is reduced and the brightness correspondingly increase. Of course, if the electron beam is focussed too much we have the opposite situation as discussed. There is an optimum focusing for optimum matching.

To find this optimum we use the particle beam parameters

$$\sigma^2_{\mathrm{b},x,y} = \epsilon_{x,y}\beta_{x,y} \qquad \text{and} \qquad \sigma^2_{\mathrm{b},x',y'} = \frac{\epsilon_{x,y}}{\beta_{x,y}}\,, \tag{101}$$

where $\beta_{x,y}$ is the betatron function at the photon source location. Including diffraction limits, the product

$$\sigma_{\mathrm{tot},x}\sigma_{\mathrm{tot},x'} = \sqrt{\epsilon_x\beta_x + \tfrac{1}{2}\,\sigma_r^2}\,\sqrt{\frac{\epsilon_x}{\beta_x} + \tfrac{1}{2}\,\sigma_{r'}^2} \tag{102}$$

has a minimum ($\frac{\mathrm{d}}{\mathrm{d}\beta_x}\sigma_{\mathrm{tot},x}\sigma_{\mathrm{tot},x'} = 0$) for

$$\beta_x = \frac{\sigma_r}{\sigma_{r'}} = \frac{L}{2\pi}\,. \tag{103}$$

The same optimum occurs for the vertical betatron function at the source point. The optimum value of the betatron functions at the source point depends only on the length of the undulator.

The values of the horizontal and vertical betatron functions should be adjusted according to (103) for optimum photon beam brightness. In case the particle beam emittances are much larger than the diffraction limited photon beam emittance, this minimum is very shallow and almost nonexistent in which case the importance of matching becomes irrelevant. As useful as matching may seem to maximize the photon beam brightness it is not always possible to perform that matching because of limitations in the storage ring focusing system. Furthermore it is practically impossible to get a perfect matching for bending magnet radiation since the effective source length L is very small, $L = 2\rho/\gamma$.

9.2 Spatial Coherence of Undulator Beams

Some fraction of a photon beam is spatially coherent depending on the actual compared to diffraction limited phase space distribution. The expression

$$\frac{\dot{N}_{\mathrm{coh}}}{\dot{N}_{\mathrm{ph}}} = \frac{\lambda^2}{16\pi^2\sigma_{\mathrm{t},x}\sigma_{\mathrm{t},x'}\sigma_{\mathrm{t},y}\sigma_{\mathrm{t},y'}} \tag{104}$$

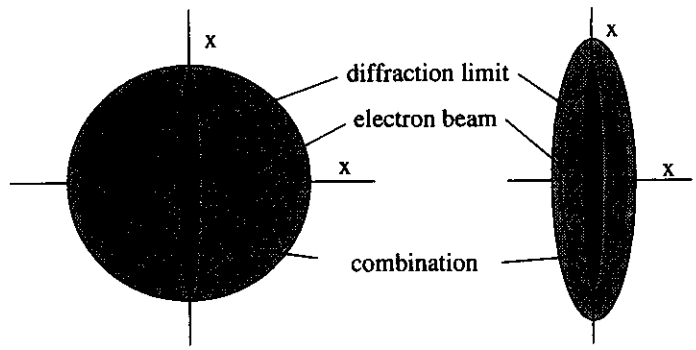

Figure 23: Matching of electron beam to diffraction limit for maximum photon beam brightness

defines that fraction of spatially coherent photon flux. Significant spatial coherent radiation is emitted into the forward direction from electron beams with an emittance of $\epsilon_u < \lambda/(4\pi)$.

10 Temporal Coherent Synchrotron Radiation

Synchrotron radiation is emitted into a broad spectrum with the lowest frequency equal to the revolution frequency and the highest frequency not far above the critical photon energy. Detailed observation of the whole radiation spectrum, however, may reveal significant differences to these theoretical spectra at the low frequency end. At low photon frequencies we may observe an enhancement of the synchrotron radiation beyond intensities predicted by the theory of synchrotron radiation as discussed so far. We note from the definition of the Poynting vector that the radiation power is a quadratic effect with respect to the electric charge. For photon wavelengths equal and longer than the bunch length, we expect therefore all particles within a bunch to radiate coherently and the intensity to be proportional to the square of the number N_e of particles rather than linearly proportional to N_e, as is the case for high frequencies. This quadratic effect can greatly enhance the radiation since the bunch population can be from 10^8 to 10^{11} electrons.

Generally such radiation is not emitted from a storage ring beam because radiation with wavelengths longer than the vacuum chamber dimensions are greatly damped and will not propagate along a metallic beam pipe. This radiation shielding is fortunate for storage ring operation since it eliminates an oth-

erwise significant energy loss mechanism. Actually, since this shielding affects all radiation of sufficient wavelength both the ordinary synchrotron radiation and the coherent radiation is suppressed.

New developments in storage ring physics, however, may make it possible to reduce the bunch length by as much as an order of magnitude below presently achieved short bunches of the order of 10 mm. Such bunches would then be much shorter than vacuum chamber dimensions and the emission of coherent radiation in some limited frequency range would be possible. Much shorter electron bunches of the order of 1 - 2 mm and associated coherent radiation can be produced in linear accelerators, and specifically with bunch compression a significant fraction of synchrotron radiation is emitted spontaneously as temporal coherent radiation.

To discuss the appearance of temporal coherent synchrotron radiation, we consider the radiation emitted from each particle within a bunch. The radiation field at a frequency ω from a single electron is

$$\mathcal{E}_k \propto \mathrm{e}^{\mathrm{i}(\omega t+\varphi_k)}, \tag{105}$$

where φ_k describes the position of the k-th electron with respect to the bunch center. With z_k the distance from the bunch center the phase is

$$\varphi_k = \frac{2\pi}{\lambda} z_k . \tag{106}$$

Here we assume that the cross section of the particle beam is small compared to the distance to the observer such that the path length differences from any point of the beam cross section to observer are small compared to the shortest wavelength involved.

The radiation power is proportional to the square of the radiation field and summing over all electrons we get

$$\begin{aligned} P(\omega) \quad &\propto \quad \sum_{k,j}^{N_e} \mathcal{E}_k \mathcal{E}_j^* \propto \sum_{k,j}^{N_e} \mathrm{e}^{\mathrm{i}(\omega t+\varphi_k)} \mathrm{e}^{-\mathrm{i}(\omega t+\varphi_j)} \\ &= \quad \sum_{k,j}^{N_e} \mathrm{e}^{\mathrm{i}(\varphi_k-\varphi_j)} = N_e + \sum_{k\neq j}^{N_e} \mathrm{e}^{\mathrm{i}(\varphi_k-\varphi_j)} . \end{aligned} \tag{107}$$

The first term N_e on the r.h.s. of (107) represents the ordinary incoherent synchrotron radiation with a power proportional to the number of radiating particles. The second term averages to zero for all but long wavelengths. The actual coherent radiation power spectrum depends on the particular particle distribution in the bunch. For a storage ring bunch it is safe to assume a gaussian particle distribution and we use therefore the density distribution

$$\Psi_g(z) = \frac{N_e}{\sqrt{2\pi}\sigma} \exp\left(-\frac{z^2}{2\sigma^2}\right), \tag{108}$$

where σ is the standard value of the gaussian bunch length. Instead summing over all electrons we integrate over all phases. Folding the density distribution (108) with the radiation power (107) we get with (105)

$$P(\omega) \propto N_e + \frac{N_e(N_e-1)}{2\pi\sigma^2} I_1 I_2 , \tag{109}$$

where the integrals I_1 and I_2 are defined by

$$I_1 = \int_{-\infty}^{\infty} \exp\left(-\frac{z^2}{2\sigma^2} + \mathrm{i}\,2\pi\,\frac{z}{\lambda}\right) \mathrm{d}z, \tag{110}$$

$$I_2 = \int_{-\infty}^{\infty} \exp\left(-\frac{w^2}{2\sigma^2} + \mathrm{i}\,2\pi\,\frac{w}{\lambda}\right) \mathrm{d}w , \tag{111}$$

and $z = \lambda\varphi_k/2\pi$ and $w = \lambda\varphi_j/2\pi$. The factor $(N-1)$ reflects the fact that we integrate only over different particles. Both integrals are equal to the Fourier transform for a gaussian particle distribution. With

$$\int_{-\infty}^{\infty} \exp\left(-\frac{z^2}{2\sigma^2} + \mathrm{i}\,2\pi\,\frac{z}{\lambda}\right) \mathrm{d}z = \sqrt{2\pi}\,\sigma \exp\left(-2\pi^2\,\frac{\sigma^2}{\lambda^2}\right) \tag{112}$$

we get from (109) for the total radiation power at the frequency $\omega = 2\pi/\lambda$

$$P(\omega) = p(\omega)\,[N_e + N_e\,(N_e-1)\,g^2(\sigma)] , \tag{113}$$

where $p(\omega)$ is the radiation power from one electron and the Fourier transform

$$g(\sigma) = \exp\left(-2\pi^2\,\frac{\sigma^2}{\lambda^2}\right) \tag{114}$$

becomes with the effective bunch length

$$\ell = \sqrt{2\pi}\sigma , \tag{115}$$

finally

$$g(\ell) = \exp\left(-\pi\,\frac{\ell^2}{\lambda^2}\right) . \tag{116}$$

The coherent radiation power falls off rapidly for wavelengths as short or even shorter than the effective bunch length ℓ.

In Fig. 24 the relative coherent radiation power is shown as a function of the effective bunch length in units of the radiation wavelength. The fast drop off is evident and for an effective bunch length of about $\ell \approx 0.6\lambda$ the radiation power is reduced to about 10% of the maximum power for very short bunches, $\ell \to 0$.

Particle beams from a linear accelerator have often a more compressed particle distribution of a form between a gaussian and a rectangular distribution. If we take the extreme of a rectangular distribution

$$\Psi_r(z) = \begin{cases} -0.5 & \text{for } < z < 0.5 \\ 0 & \text{otherwise} \end{cases} \tag{117}$$

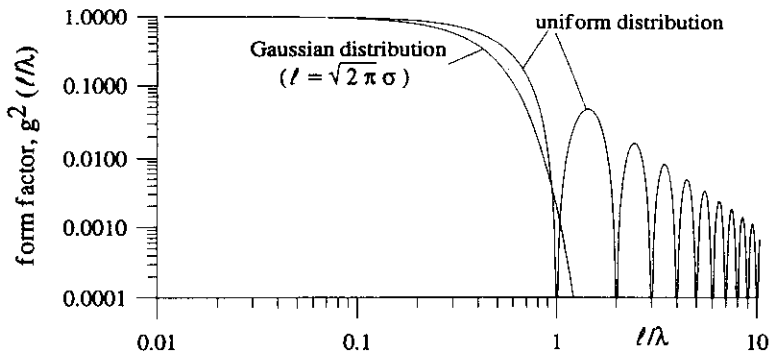

Figure 24: Coherent synchrotron radiation power spectrum $g^2(\ell)$ as a function of the bunchlength ℓ

we expect to extend the radiation spectrum since the corners and sharp changes of the particle density require a broader spectrum in the Fourier transform. Following the procedure for the gaussian beam we get for a rectangular particle distribution the Fourier transform

$$g(\ell) = \frac{\sin x}{x}, \tag{118}$$

where $x = \pi(\ell/\lambda)$. Fig. 24 also shows the relative coherent radiation power for this distribution and we note a significant but scalloping extension to higher radiation frequencies.